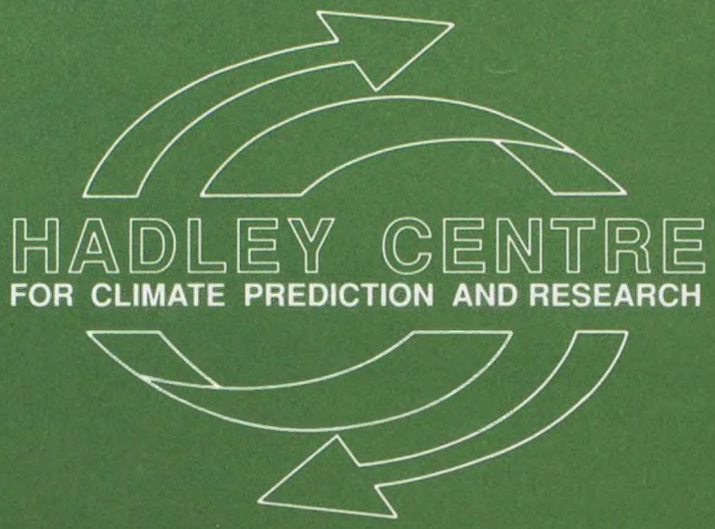

ENSO responses and low frequency weather variability in the North Pacific/American sector 1949-93

by

A C Renshaw, D P Rowell and C K Folland

CRTN 73

August 1996

CLIMATE
RESEARCH
TECHNICAL
NOTE

Hadley Centre
Meteorological Office
London Road
Bracknell
Berkshire RG12 2SY

CLIMATE RESEARCH TECHNICAL NOTE NO. 73

ENSO RESPONSES AND LOW FREQUENCY WEATHER VARIABILITY IN THE NORTH PACIFIC/AMERICAN SECTOR 1949-93

by

A C Renshaw, D P Rowell and C K Folland

Hadley Centre for Climate Prediction and Research
Meteorological Office
London Road
Bracknell
Berkshire RG12 2SY

NOTE: This paper has not been published. Permission to quote from it should be obtained from the Director of the Hadley Centre.

ABSTRACT

A study of the impact of ENSO in the Hadley Centre's atmospheric climate model (HADAM1) is presented, with emphasis on the North Pacific American (NPA) sector. The study is based on an ensemble of 6 integrations for the period 1949-93, forced with observed global sea-ice and sea surface temperature data (GISST).

From seasonal composite analyses, the model is shown to reproduce most of the known features of the worldwide atmospheric response to ENSO; it also highlights additional areas that are sensitive to ENSO, but too weakly to be identified from the observed record alone. Although there is considerable variability in the response to individual ENSO events, our results indicate that the underlying signal is approximately linear in both model and nature.

Focusing on the NPA sector, the leading modes of low frequency weather variability for the winter season January to March (JFM) are identified on their natural timescales for both the modelled and observed atmospheres. These modes are analyzed via rotated EOF analysis of *daily* 500 hPa height data, filtered to remove synoptic timescale variations. The model gives a skilful simulation of the main features of the four leading modes in the NPA region: the Pacific North American (PNA), the West Pacific (WP), the East Pacific (EP), and the North Pacific (NP) modes. The sensitivity of these modes to SSTs is investigated. In particular, sensitivity to SSTs associated with ENSO is analyzed in terms of the shift in frequency of occurrence of the opposing phases of a mode between warm event (El Nino) and cold event (La Nina) years. Three of the observed modes show such a sensitivity: the PNA, WP and NP modes. Of the corresponding model modes, only the PNA responds correctly to ENSO, clearly illustrated by changes in both the frequency and duration of PNA episodes between warm and cold event years. The EP mode shows no sensitivity to ENSO, in either model or observed atmospheres. Finally, although the model is able to reproduce the pattern of decadal anomalies seen in the North Pacific in the years 1977-87, which is related to the prevalence of the positive phase of the PNA in this period, it does so with a much reduced amplitude. Possible reasons for this discrepancy are discussed.

1. Introduction

In the 100 years since its discovery (Hildebrandsson 1897), the southern oscillation has been the subject of much interest and research. Following the work of Bjerknes (1969) we now understand the southern oscillation to be intimately linked with the cycle of warm (El Nino) and cold (La Nina or El Veijo) sea surface temperature (SST) anomalies in the equatorial Pacific, part of a complex ocean-atmosphere interaction usually termed ENSO (El Nino Southern Oscillation). For ease of reference we shall use the term ENSO to encompass both extremes of the tropical Pacific cycle, which we shall refer to separately as warm and cold events. The interest in ENSO stems from its importance to weather patterns throughout the globe. Such teleconnections were first recognised by Walker (1924), and have been explored in many subsequent papers, the 1980s being a particularly prolific decade for such research (e.g. Horel and Wallace 1981, Pan and Oort 1983, Ropelewski and Halpert 1987 and 1989, Kiladis and Diaz 1989 and many others). One extratropical area which stands out from these studies as having a strong, consistent ENSO response is the North Pacific/American (NPA) sector, where a characteristic pattern of anomalies is found to recur in ENSO years: the so-called Pacific North American (PNA) pattern. The response of NPA modes of low frequency weather variability is a particular focus of this paper.

Alongside the observational studies, a growing body of work focused on the response of atmospheric general circulation models (AGCMs) to imposed SST anomalies in the tropical Pacific. These studies ranged from those using idealized anomalies (e.g. Rowntree 1972), or a composite warm event anomaly (e.g. Blackmon et al 1983, Shukla and Wallace 1983), to multi-year integrations with observed SSTs (e.g. Lau 1985) which allowed the evolution of ENSO events to be followed. In recent years the need to perform such integrations in ensemble mode has been increasingly recognised (e.g. Barnett et al 1994, Smith 1995), so that SST-forced signals in the extratropics might be better distinguished from the noise of the internal atmospheric variability. In general such modelling studies have given reasonable simulations of the global response to warm events, including the PNA response, although some studies looking separately at cold events have been less successful (e.g. Cubasch 1985). Recent multi-year integrations have been able to capture some aspects of the so-called 'climate shift' seen in the North Pacific in the late 1970s / early 1980s (e.g Graham et al 1994) which involved large temperature anomalies over North America, and which has been related to changes in ENSO. The ability to understand the origin of such regional variations is particularly important in the light of current interest in the detection of anthropogenic climate change. The ability to simulate the atmospheric response to tropical Pacific SSTs is also of great importance to seasonal forecasting, especially as the skill in predicting these SSTs has increased considerably in recent years (Barnston 1995).

While AGCMs can provide us with a realistic atmosphere in which to investigate the mechanisms linking warm and cold events to the extratropics, this verisimilitude, and hence complexity, also makes such investigation difficult. Insight into these mechanisms has more usually been gained through the use of more simplified models. For example the work of Hoskins and Karoly (1981), later extended by Sardeshmukh and Hoskins (1988), provided a framework for understanding the PNA response to warm and cold events. Warm SST anomalies in the tropical Pacific enhance local precipitation and give rise to upper level divergence; advection of vorticity by the divergent flow gives an effective Rossby wave generator in the western subtropical Pacific. Wave trains emanating from this region carry

energy into the extratropics in a great circle path, which, in the northern hemisphere, arches over the North Pacific and North America to give the PNA-like pattern in the mid-latitude jet stream. Other studies have indicated that the associated shifts in storm track positions in warm and cold events, and consequent changes in transient vorticity fluxes, also have an important role in maintaining the extratropical teleconnections (Held et al 1989, Lau 1988, Hoerling and Ting 1994).

The relationship between warm events and the PNA pattern is, however, less deterministic than the above discussion suggests. Strong PNA patterns are produced in non-ENSO years both in observed atmospheres and in modelled atmospheres forced with observed SSTs, while a strong warm or cold event does not always give the expected PNA response. Moreover the PNA pattern is identified as a preferred mode of variability in AGCMs forced with climatological SSTs (Lau 1981, Chervin 1986). These results indicate that the PNA mode is a natural mode internal to the atmosphere, and that the effect of a warm or cold event is to bias the probability that the PNA mode will occur in its positive or negative phase. Palmer (1993) gives a very useful discussion of this view in which Lorenz's (1963) simple model of a non-linear system provides an analogy for the chaotic extratropical circulation. The two 'wings' of the system's attractor represent two distinct weather regimes, between which transitions occur at random intervals, but which in the long term are equally likely states for the system. Palmer shows that if a linear oscillator, representing the tropical atmosphere, is coupled to the Lorenz model, the effect is not to alter the phase space location of the two regimes, but rather to alter their relative population density. The system remains chaotic, and transitions between regimes still occur. Such behaviour corresponds well to the PNA response to ENSO seen in modelling (Molteni et al 1990) and observed (Livezey and Mo 1987) studies.

It is with this theoretical framework in mind that we approach the analysis of the response to ENSO seen in multi-decadal atmospheric simulations, and in the observed record. We use a 6 member ensemble of integrations, forced with observed SSTs and sea-ice data, to give a thorough analysis of our model's skill in simulating the response to ENSO, and to address the question of the linearity of response to warm and cold events. Focusing on the NPA sector, the leading modes of low frequency weather variability are identified. The ensemble provides the opportunity to evaluate the relative importance of SSTs to the variability of each of the NPA modes. These modes are identified on their natural timescales, by analysis of daily data, low pass filtered to remove synoptic timescale variations. This allows the influence of ENSO on the frequency of occurrence of the modes to be investigated, and any shift in probability distributions, as suggested by Palmer (1993), to be identified. This would not be possible with an analysis of monthly or seasonal data.

The paper is arranged as follows. A brief description of the model and experimental design is given in section 2. In section 3, the skill of the model in simulating the seasonal mean response to ENSO is assessed, by comparing model and observed composites for warm and cold events. Global composites of pressure at mean sea level, surface air temperature and precipitation are discussed for each of four standard seasons; composites for the NPA region in the winter season JFM are more closely studied. In section 4, the leading modes of variability in the NPA region are identified using rotated EOF analysis. Model and observed modes of variability are compared. For each of the modes, the influence of warm and cold events is assessed in terms of the shift in population distribution . The influence on duration

of events is also studied for the PNA mode. Finally, in section 5, we present some discussion and conclusions.

2. Methodology

a) Model Formulation

All integrations described in this paper use the first version of the HADley Centre Atmospheric Model, known as HADAM1. HADAM1 is a grid-point model with a horizontal resolution of 2.5° latitude by 3.75° longitude and 19 hybrid levels in the vertical. Boundary layer processes are represented on the lowest 5 levels. There is also a four level soil model determining heat transport, and a single layer model for surface hydrology. The model calculates cloud amounts (convective and large scale) and cloud liquid water and ice contents. The radiation scheme, which resolves six short-wave and four long-wave bands, responds to these cloud variables. The atmospheric carbon dioxide concentration is fixed at 321 ppmv, while ozone varies with season and latitude. HADAM1 is the model submitted in 1993 by the UK Meteorological Office to the Atmospheric Model Intercomparison Project, and a full description of its physics and dynamics is given in Phillips (1994). Rowell (1996) provides a discussion of the skill of its global climatology.

b) Experimental design and data

Model results in this paper are based on an ensemble of six, multi-decadal integrations forced with observed SSTs: the same set of experiments analyzed in Rowell (1996) and Davies et al (1996). Each integration was started at 00Z on 1 October 1948, using its own, unique set of initial conditions, selected from recent UK Meteorological Office operational analyses for early October. Initial values of soil moisture and snow depth were provided from an adaptation of Willmott et al.'s (1985) climatologies, while deep soil temperatures were initialized using equations given in Warrilow et al. (1986). After initialization, heat and moisture contents over the land surface were free to interact with the model atmosphere. As the model atmosphere takes some time to adjust from its initial state to one in quasi-equilibrium with the historic SSTs, the first two months of the integration were discarded. The integrations were run on to 00Z on 1 December 1993, giving 45 complete years for analysis.

The runs were forced throughout by observed data from the GISST (Global sea-Ice and Sea Surface Temperature) data set, version 1.1 (Parker et al. 1995). GISST provides globally complete, monthly mean fields of SST and sea-ice data on a 1° by 1° grid (calculated by projecting 5^0 SST anomalies onto a 1° climatology). Grid points are either set to ice-covered or ice-free. The SSTs were interpolated to the larger model grid by taking the area-weighted average of temperatures in non-ice 1° squares; where ice cover exceeded 50%, model grid-boxes were designated as ice points. Finally, the monthly SST and sea-ice data were interpolated to pentad values to provide a smoother boundary forcing to the model atmosphere.

Several observed data sets are used in this paper to assess the model performance. Observed mean sea level pressure (MSLP) data were taken from an the latest version (2.1) of the Basnett and Parker (1995) data set, which is a quality controlled blend of existing gridded data sets. The surface air temperatures used are a blend of land air temperature data

from the Climate Research Unit, University of East Anglia (Jones 1994), and night marine air temperature data, much as described by Bottomley et al (1990), though since improved as described in Parker et al (1995). Gridded precipitation data (for land areas only) were an updated version of the data set described in Hulme (1994). 500hPa height data (seasonal and daily data) were taken from the U.K. Meteorological Office archive (Jackson 1986).

3. Modelling the Mean Response to ENSO

In this section we analyze the skill of the HADAM1 model in simulating the global atmospheric response to warm and cold events in the tropical Pacific. We consider first the model's skill in simulating the Southern Oscillation Index (SOI), then investigate the global response in each of the four standard seasons, looking at surface variables of MSLP, temperature and precipitation. We then focus on one of the extratropical regions most strongly affected by tropical Pacific SSTs: the Pacific North American sector.

a. Modelling the SOI

The SOI is widely used as a measure of the tropical atmospheric changes associated with warm and cold events (Ropelewski and Jones 1987). The index shown in fig.1 is the (Tahiti minus Darwin) MSLP difference calculated from 5 month running mean values of normalised monthly anomalies (wrt 1951-80). The SOI values of the 6 model runs are in very good agreement, indicating a strong SST-forced component. Given an ensemble of runs with a common forcing, the "analysis of variance" technique allows us to assess the fraction of variance, ρ, attributable to that forcing; the remaining variance being the result of random variations internal to the atmosphere. Details of the technique are given in Rowell et al (1995). For the SOI shown in fig.1, the oceanic forcing explains 86% of the variance (with 95% confidence limits of 81% and 90% [calculated as in Rowell 1996]).

Even if the model were perfect, the expected correlation between the ensemble mean and the observed SOI would be less than one, since both time series are subject to random variations. The expected correlation, $r_{EM,crit}$, between the ensemble mean and a further model run is easily calculated from ρ (Rowell 1996); and this provides an upper limit against which model/observed correlations may be assessed. For the SOI in fig.1, the correlation between the ensemble mean and observed values is 0.85, which is close to the $r_{EM,crit}$ of 0.92; thus the SOI is skilfully simulated. However the model SOI does have a slight positive bias in more recent years, such that the response is too strong in the 1985 cold event, and too weak in the 1982/83 and 1987 warm events. This bias has also been seen in other modelling studies (e.g. Konig et al 1990, Latif et al 1990, Smith 1995, Livezey et al 1995). This could be due to errors in the forcing SST data, or in the verifying MSLP data, or could possibly reflect a common error in the models' response, at Tahiti and/or Darwin, to the global SST forcing over this period.

b. Global response to ENSO - composite methodology

In order to compare the modelled and observed responses to ENSO throughout the globe, seasonal composites have been created for MSLP, surface air temperature and precipitation. For each season, the years of the integration (1949-93) were ranked in order of the mean SST in the Nino3 region [5°N-5°S,90°-150°W] and the top quartile, i.e the 11

warmest years, averaged to give the 'warm event' composite; similarly the average of the 11 coldest years gave the cold event composite. Composites are based on tropical Pacific SSTs, rather than the SOI index, because this gives a more direct insight into the influence of the boundary forcing. In previous composite studies, such as Kiladis and Diaz (1989) (hereafter KD) or Ropelewski and Halpert (1987), an ENSO year, year(0), is first identified, and seasonal composites then created from year(-1) through to year(+1). In our analysis years are selected for each season independently since events do not all follow the same evolution (in recent years in particular the usual cycle of alternate warm and cold events has not been followed). However, our results can be compared with KD composites for DJF and MAM in year(+1), and for JJA and SON in year(0). The years contributing to each seasonal composite are listed in Table 1.

TABLE 1. Years used to create warm and cold event composites. [DJF: year given is that of the December]

	DJF	MAM	JJA	SON
Warm Events	51,57,65,68, 69,72,76,82, 86,87,91	53,57,58,65, 69,72,83,87, 91,92,93	51,57,63,65, 69,72,76,82, 83,87,91	51,57,63,65, 69,72,76,82, 86,87,91
Cold Events	49,54,55,62, 64,67,70,73, 75,84,88	50,54,55,56, 62,64,67,68, 71,85,89	49,54,55,64, 70,71,73,75, 78,85,88	49,54,55,61, 64,67,70,71, 73,75,88

In calculating observed composite values, data were required in at least half of the designated warm (or cold) years. Model composites were formed from ensemble mean values, thus compared with observed composites their signal-to-noise ratio is higher and areas of significant difference more extensive. Significant areas may be identified with a two-tailed t-test, but the sample size must be reduced to account for possible serial correlation from one selected event to another. Assuming a Markov process, the effective number of points in a time series, n_e, can be approximated as follows:

$$n_e \approx \frac{n_0(1-r[1])}{(1+r[1])}$$

where n_o is the actual number of points and r[1] the lag-1 correlation coefficient (WMO 1966). Since the years selected for each composite are not generally consecutive, n_e provides a lower estimate for the effective sample size; the significance calculated, using n_e, thus tends to be conservative.

To calculate the significance of warm - cold composite differences the t statistic is calculated as follows (e.g. Zwiers and von Storch 1995) :-

$$t = \frac{\overline{X_1} - \overline{X_2}}{S(1/n_{e1} + 1/n_{e2})^{1/2}}$$

where $\overline{X_1}$ ($\overline{X_2}$) = warm (cold) event seasonal mean

n_{e1} (n_{e2}) = effective sample size in warm (cold) years

and S= estimate of the standard deviation of the population sampled, (in this case the standard deviation of all seasonal values 1949-93). The probability of such a value occurring by chance is then found from the t-statistic, using (n_{e1}+n_{e2}-2) degrees of freedom.

c. Global Composite Response to ENSO - MSLP

Warm and cold event MSLP composites have been calculated for model and observed data. The warm minus cold event composite differences are shown in fig.2. In all seasons the tropical response to ENSO is well simulated, consistent with the good simulation of the SOI. In the extratropics, most significant features of the observed composite differences are also well simulated, although with some discrepancies as to their strength and exact location. The most obvious regional difference in all seasons is the simulation of a strong positive centre west of the Antarctic peninsula, which is much weaker, or absent, in the available observations. A measure of the model's skill in simulating the atmospheric response to ENSO is provided by the area weighted spatial correlations between modelled and observed composite differences, listed in table 2.

Warm and cold seasonal composite anomalies (with respect to the mean of all years 1949-93) have also been studied, to identify any non-linear response to NINO3 SSTs. We find that both model and observed analyses show an approximately linear response to ENSO in those areas where composite anomalies are significant. As previously mentioned, much of the random variation is averaged out when calculating ensemble mean composites, thus the signal-to-noise ratio is increased in comparison to observed composites. Regions showing a significant ENSO response are thus more extensive in the ensemble mean composites, and the warm and cold event composites are therefore more exact mirror images than their observed counterparts. However, correlations between warm and cold event composites for individual model runs (Table 3) indicate that the model response is no more linear than that found in nature.

The main features of the seasonal composite differences shown in fig.2 are discussed below.

1) DJF

The pattern of observed composite difference, fig.2a, agrees well with previous analyses such as van Loon (1986) and Barnett (1988). The most extensive areas of significant difference are in the tropics. Here, the largest anomalies, sited in the western tropical Pacific, take the form of two anomalous anticyclonic centres straddling the equator. Significantly increased pressure also encompasses most of Australia, the tropical Atlantic and Indian oceans, and much of Africa. Decreased pressure prevails in the eastern tropical Pacific and the Gulf of Mexico. The model composite difference, fig.2b, captures the spatial distribution of the tropical anomalies well (table 2) although their strength is generally too great, in particular over Indonesia.

A feature familiar from observational and modelling studies (e.g. Lau and Nath 1994, Graham et al 1994) is the large decrease in pressure in the North Pacific centred near the Aleutian Islands. The model captures the strength of this feature well, but positions it too far

east. The model shows a band of significantly lowered pressure at around 50 S, also present, but not significant, in our observed analysis and seen in those of van Loon (1986) and Karoly (1989).

Fig.3 shows the composite anomalies for warm and cold events separately, demonstrating the general linearity of the response to ENSO (see spatial correlations in table 3). However, the North Atlantic appears to be one region with a nonlinear sensitivity to ENSO. In warm event years there is good agreement between observed and modelled composites, and although the observed anomalies do not achieve significance, the ensemble mean anomalies are significant over much of the North Atlantic. Our warm event anomaly pattern in this region shows increased pressure near Iceland and reduced pressure in the midlatitude North Atlantic, corresponding to increased blocking in the North Atlantic (low phase of the North Atlantic Oscillation); this is consistent with the patterns identified by Rogers (1984) and Fraedrich and Muller (1992). In cold event years however, observed anomalies are weaker and significant ensemble mean anomalies less extensive than in the warm event composite. Moreover there is little agreement between observed and modelled anomaly patterns. This suggests that the North Atlantic region is more sensitive to warm than to cold events, as seen in Davies et al (1996) when looking at 500 hPa height.

2) MAM

Observed and modelled MSLP composite differences for this season are shown in figs. 2c and 2d respectively. Tropical anomalies are similar to those in DJF, but the area of high pressure over the Indian ocean extends further north into India. Again the model's simulation of the pattern is good, [see table 2] but anomalies are too strong, particularly in the western tropical Pacific.

In the extratropics many features are common to both modelled and observed analyses. There is a significant lowering of pressure across the whole of the extratropical North Pacific, extending into the west coast of the U.S., while an area of increased pressure lies over central and eastern Canada. Australia is encompassed by the southerly of two anomalous anticyclonic centres in the western Pacific, while a large area of low pressure lies to the south-east of New Zealand.

Some extratropical features are significant only in the ensemble mean analysis: an elongated area of low pressure over Eastern europe through central Asia; a region of low pressure to the south of Africa; as well as the positive centre to the west of the Antarctic peninsula. The sign of the observed composite differences in these regions is consistent with that seen in the model, and so the model may be revealing real, but weak, responses to ENSO.

3) JJA

Observed and modelled MSLP composite differences are shown in figs. 2e and 2f respectively. As in the other seasons the model gives a good simulation of tropical anomalies (see table 2), with reduced pressure in the east and increased pressure in the west of the tropical Pacific. Both model and observed analyses also show a significant increase in pressure in the Middle East and over much of the tropical Atlantic.

The strong seasonality of the response to ENSO is demonstrated by the few areas of significant difference seen in the northern extratropics compared to DJF. In the southern hemisphere, including the extratropics, significant features are more prevalent. The observed analysis, which agrees well with that of van Loon (1986), shows a large positive anomaly over Australia, at a maximum over South Australia, and a strong negative anomaly in the eastern Pacific, centred in model and observations near 40°S. The model simulates the latter centre well, but the former is poorly reproduced, with the anomaly over southern Australia of the wrong sign. The model's strong positive centre to the west of the Antarctic peninsula is only hinted at in the observations, but does appear more strongly in van Loon's (1986) analysis.

4) SON

Observed and modelled MSLP composite differences for this season are shown in figs. 2g and 2h respectively. In general the simulation of the tropical response to ENSO is good, although the model has a stronger pressure increase in the Indian ocean. The model also shows an apparently erroneous area of significantly reduced pressure to the south-east of Japan. The simulation in the extratropics is rather poor in both hemispheres, making this the poorest seasonal simulation. The model fails, for example, to produce the observed increase in pressure over central and north-west Canada. However, patterns over the oceans are somewhat better simulated.

As in the other seasons, the model and observed response to ENSO is linear where it is significant.

d. Global Composite Response to ENSO - Surface air temperature

Composite differences have also been calculated for observed and modelled surface air temperature. As for MSLP, the agreement between modelled and observed large scale patterns is generally good; not only over the oceans, which we expect given the SST forcing, but also over many land areas (spatial correlations between observed and modelled analyses are given in table 2). Again, as for MSLP, the response to ENSO is approximately linear in those regions where any significant response is detected (table 3). The warm minus cold composite difference responses are discussed below for each season; for reasons of space the composites are not shown.

1) DJF

Consistent with earlier studies (e.g. KD, Ropelewski and Halpert (1986)), our observed composite difference for this season shows a strong warming over Alaska/western Canada, and along the west coast of the U.S., together with cooling over the south-eastern U.S. The model simulates these features well, although the warming over Canada, while significant, is insufficiently strong (maximum temperature difference 2.0°C compared to 2.7°C in the observed analysis). India, east Africa and northern South America are among the tropical areas correctly simulated by the model as significantly warmer. The model also shows significant cooling over New Zealand, which is consistent with the observations.

2) MAM

Our observed composite difference is in good agreement with that of KD, showing warm anomalies in many tropical areas and in Canada; and below normal temperatures in the southern U.S, and New Zealand. The model captures all these observed features well, although, as in DJF, the Canadian warming is rather weak. Halpert and Ropelewski (1992) describe a non-linear response in western Europe involving a decrease in temperature in cold event years, but no response in warm event years. We find no significant influence on European temperature in either phase of ENSO, in either model or observations; moreover, in cold event years the model and observed analyses disagree as to the sign of the anomaly over Europe.

3) JJA

The model composite difference correctly simulates significantly warmer anomalies over India and central Africa, and cold anomalies over northern Australia and around New Zealand, although the model temperature differences around New Zealand are less than half of the 1°C differences seen in the observations. The model also has significantly cooler conditions around Japan, and in the eastern U.S./ Canada: features also identified by KD, and present, but not significant, in our observed analysis.

4) SON

Major features in the model and observed analyses are in good agreement and are generally supported by the analysis of KD. All indicate warming over Alaska, and cooling over eastern Canada; although the model's region of cooling is too small. Many tropical areas show warming, including India, Indonesia, central Africa and central America. Northern Australia and New Zealand have below normal temperatures, while south-eastern Australia is warmer than usual. KD noted significantly colder temperatures over the U.K. and Spain in this season; our analyses also have negative anomalies in this region (in each case composite differences of around -0.5°C), but they are significant only over a few points to the west of Spain.

e. Global Composite Response to ENSO - Precipitation

Since our data set of observed gridded precipitation is confined to land areas (Hulme 1994), and existing ocean data sets are too short for use in this study, some of the largest composite differences seen in the model cannot be confirmed. However, where observed data are available, model and observed analyses are generally in agreement, although observed values are rarely significant at the 95% level. Further support for our model precipitation responses is provided by KD and Ropelewski and Halpert (1986/7). As for surface air temperature and MSLP, the ENSO response is approximately linear (table 3).

Some model anomalies appear in all seasons, for example a band of increased rainfall close to the equator in the central and eastern Pacific. The largest anomalies in this band (over 7.5 mm/day in DJF) are situated just east of the dateline. Also common to all seasons are decreases in rainfall over Indonesia, the northern Indian ocean and the Indian continent. Northern Australia and New Zealand also experience dry conditions in all seasons, as does

northern South America, particularly in DJF. The observed rainfall anomalies, where available, are in support of these model signals. Other areas experience anomalous rainfall only in certain seasons. The warm minus cold composite differences are discussed below, again, for reasons of space, the composites are not shown.

1) DJF

The model composite difference shows that while Canada and Alaska are drier than normal, the U.S. is wetter, significantly so along the west coast and in the south-east. Other land areas experiencing anomalously wet conditions include Spain and Argentina. The observed composite differences, although not significant, are consistent with the modelled values in these areas. The South American and the south-east U.S. responses are also shown by Ropelewski and Halpert (1986) and KD, and the latter also confirm the precipitation signal over Spain.

2) MAM

The model composite difference reveals significantly wetter conditions in the southern U.S., as noted by Ropelewski and Halpert (1986) and KD. Southern Africa also shows a significant response with decreased rainfall . The region of dry conditions over northern South America, seen in all seasons, now extends to the north-east tip of Brazil. As in DJF, Argentina experiences significantly increased precipitation. The observed composite differences are consistent with the model analysis, although only over the south-eastern U.S. are values significant.

3) JJA

In addition to the anomalies common to all seasons, the model composite difference shows the central U.S., and central South America are significantly wetter than normal; the latter response is also noted by Ropelewski and Halpert (1986). Observed composites are weaker, and not significant, but are consistent with the modelled values.

4) SON

The model composite reveals that significantly wetter than normal conditions prevail over the north-eastern Pacific, extending over south-western U.S.. KD and Ropelewski and Halpert (1986) confirm the increase in rainfall in the great basin region, which is also represented (though not significant) in our observed analysis.

TABLE 2. Weighted spatial correlation between modelled and observed composite differences (Warm minus cold events) calculated on the model grid (3.75°x2.5°). Tropical correlations are for the region 25°N to 25°S. The North Pacific American (NPA) sector is the area 20°N-85°N, 50°W-120°E. Precipitation correlations are over land areas only (~25% of the globe) due to limited observational data coverage.

	DJF	MAM	JJA	SON	JFM
Global MSLP	0.66	0.63	0.54	0.43	
Global Temp	0.58	0.60	0.69	0.66	
Global Precip	0.68	0.64	0.43	0.46	
Tropical MSLP	0.87	0.93	0.87	0.84	
Tropical Temp	0.71	0.71	0.79	0.71	
Tropical Precip	0.71	0.66	0.44	0.49	
NPA MSLP	0.50	0.77	0.56	0.14	0.67
NPA Temp	0.67	0.64	0.65	0.57	0.76
NPA Precip	0.52	0.50	0.10	-0.15	0.52
NPA 500 hPa	0.61	0.77	0.58	0.41	0.67

TABLE 3. Weighted spatial correlations between warm and cold event composite anomalies, taken over the globe, calculated on model (3.75°x2.5°) grid. Values for ensemble mean (EM) composites are shown as well as the average values (AV) of the 6 individual model runs.

	DJF	MAM	JJA	SON
Model MSLP (EM)	-0.92	-0.90	-0.89	-0.88
Model MSLP (AV)	-0.81	-0.75	-0.60	-0.75
Observed MSLP	-0.65	-0.77	-0.76	-0.68
Model Temp (EM)	-0.84	-0.67	-0.75	-0.77
Model Temp (AV)	-0.71	-0.59	-0.64	-0.65
Observed Temp	-0.72	-0.63	-0.67	-0.71
Model Precip (EM)	-0.86	-0.86	-0.83	-0.84
Model Precip (AV)	-0.81	-0.76	-0.71	-0.77
Observed Precip	-0.81	-0.75	-0.68	-0.78

f. ENSO Response in the Extratropical North Pacific American Sector [20°N-80°N,50°W-120°E]

The strongest extratropical ENSO response in the model and observations is in winter in the North Pacific American (NPA) sector. The remainder of the paper will focus on this region and season, since a strong signal is desirable in order to develop techniques for investigating the response of the atmosphere's natural modes to ENSO. However, instead of using the conventional months (DJF), winter will be defined as the months January to March (JFM), since we find observed and modelled composite differences are in rather better agreement in this season [see table 2]. In addition, February and March composite differences show greater consistency than those for December and January. The choice of JFM as the season most strongly influenced by SSTs is further supported by Barnston's (1994) work on predictability in the NPA sector. Years contributing to the composites are as follows:
warm events: 1958,1966,1969,1970,1973,1977,1983,1987,1988,1992,1993
cold events: 1950,1955,1956,1968,1971,1974,1975,1976,1981,1985,1989.

In section 4 we analyze the natural modes of variability in the NPA sector using 500 hPa height data. For easier comparison with that section, we show composites in the NPA sector using 500 hPa height data rather than MSLP. However, although tending to have more extensive areas of significance, composite anomalies for MSLP show very similar patterns to those of 500 hPa height, demonstrating the equivalent barotropic nature of anomalies in this region (Blackmon et al 1983). Figs. 4a and 4b show observed and modelled warm minus cold event composite anomalies of 500 hPa height for JFM for (approximately) the NPA sector. Model and observed analyses both show three strong anomaly centres: negative over the North Pacific and south-east U.S., and positive over Canada. This general pattern of response is well known from many observed and modelling studies (e.g. Horel and Wallace 1981, Chen 1982, Lau and Nath 1994). Although the model captures the general nature of the observed pattern, there are discrepancies in the location of the anomaly centres, most noticeably over the North Pacific, where the model's negative anomaly is centred too far south and east. Figs. 5a to 5d show separate warm and cold event composite anomalies, revealing an approximately inverse pattern of anomalies (see also spatial correlations - table 4). In warm event years, the anomalies are somewhat stronger and consequently the model is in rather better agreement with the observed analysis. In both extremes of ENSO, the model's response in the North Pacific has the greater magnitude; the model composites also show a more extensive area of significance than the observed (although the latter effect is largely due to taking ensemble means) .

Figs. 4c and 4d show the JFM warm minus cold composite differences for surface air temperature. Both model and observations show warming over Canada and along the western coast of the North American continent; and cooling over the south-eastern U.S., centred over Florida. These patterns are of course closely linked to the circulation changes illustrated in figs. 4a and 4b. In warm event years, the increased ridging over western Canada increases the flow of warm maritime air into the region. Storm track composites (not shown) reveal that in warm event years both modelled and observed storm tracks are shifted south, and penetrate less far into the American continent (consistent with the analysis of Lau 1988). Cloud cover over Canada is therefore reduced, further enhancing the warming along the coast, although this effect is probably offset by radiational cooling at night inland and at higher altitudes. At the same time, increased troughing in the south-east U.S. steers cold air masses southward more frequently, and there is an increase in storminess and hence cloud cover; both factors contributing to the temperature falls seen in this region. In cold event years when the flow into the Canada/Alaska region is more zonal, and there is less troughing in the south-east U.S., anomalies of reverse polarity develop. The surface air temperature composite patterns in warm and cold event years (not shown) are approximately inverse, although the agreement is rather less good than for 500 hPa height (see table 4), at least partly because of the greater spatial detail present in the former. Model anomalies are stronger than observed for both extremes of ENSO.

The warm minus cold event composite difference shown in fig.4f reveals that the model also has a strong precipitation response to tropical Pacific SSTs. The observed anomalies, where available, have the same pattern as the model, but are significant only in the far south-eastern U.S. and a small area over the Great Lakes (fig.4e). Reduced precipitation in the Alaska/Canada region is consistent with the increased subsidence and associated heating expected in this area of increased ridging. The southward shift of storm tracks in warm event years also contributes to reduced precipitation in this region. In the

south-east increased storminess and moisture advection lead to increases in precipitation. The patterns of precipitation linked with ENSO are familiar from studies such as Ropelewski and Halpert (1986) and KD. Both the precipitation and temperature patterns described above are consistent with those found to be associated with the PNA pattern by Leathers et al (1991). The response to ENSO appears to be approximately linear, with the inverse pattern appearing in cold event years (see table 4), although with somewhat reduced magnitude.

Table 4. Weighted spatial correlations between warm and cold event composite anomalies, taken over the NPA sector in season JFM

	Model	Observed
500 hPa height	-0.88	-0.80
MSLP (*not shown*)	-0.86	-0.91
Temperature	-0.62	-0.67
Precipitation	-0.82	-0.77

For all the variables discussed above, the *pattern* of response in warm event years is approximately the inverse of that in cold event years. The match is closest for the 500 hPa height and MSLP fields, for which the link with ENSO is most direct; small changes in circulation anomalies have a larger impact on the surface variables of temperature and precipitation in the NPA sector. However, in both model and observations, the *amplitude* of response is somewhat lower in the cold event composites (for 500 hPa height, the maxima of the North Pacific centre is approximately 2/3 of that in the warm event composite)*. One reason for this difference may be that the contributing warm events were slightly stronger than the contributing cold events (average NINO3 anomalies for the 11 year composites are 0.93^0C and -0.82^0C for warm and cold events respectively). Much of the difference can also be attributed to sampling problems, since there is considerable variability from one event to another, and in fact the magnitude of the 500 hPa response in the warm event composite does not differ significantly (at the 95% confidence level) from that of the cold event composite in the observed analysis; and in the model analysis does so only at the centre of the North Pacific anomaly. In spite of the considerable variation in the NPA response to different ENSO events in the season JFM, and indeed in the model response to a single ENSO event (shown by the spread of the individual ensemble members), our results are consistent with an underlying ENSO signal that is approximately linear. However, as suggested by Palmer (1988) and section 4b of this paper, the intraseasonal variability of the response to ENSO does vary between warm and cold events.

* Footnote: Note that if the warm event anomaly is strong, there is a tendency for an inverse pattern to be seen in the average of any subset of the non warm event years, such as the cold event composite, since anomalies are calculated with respect to the whole period. However, our composite anomalies are too strong to be simply an artifact of the compositing system.

4. Leading modes of winter variability in the North Pacific American sector, and their relation to SSTs.

The previous section highlighted the strong connection between ENSO and the atmosphere in the North Pacific American (NPA) sector [50°W-120°E, 20°N-85°N]. We now investigate this link in terms of the influence of warm and cold events on the leading modes of low-frequency weather variability in the NPA region.

a) Methodology and description of modes

We have chosen to identify the modes of low-frequency weather variability by performing a Rotated Empirical Orthogonal Function (REOF) analysis of 500 hPa height data in the northern hemisphere. Patterns derived by REOF analysis are more robust than their unrotated counterparts (Cheng et al 1995), and are believed to be more physically realistic, since unrotated EOFs can compound physically independent spatial patterns, when those patterns are substantially smaller than the analysis domain. In order to investigate the modes on their natural timescales, we have used daily data, low-pass filtered to remove synoptic timescale variations. Our results are therefore closer to those of Richman (1994), who also used low-pass filtered daily data, than to those of Barnston and Livezey (1987) where monthly mean fields were analyzed.

As the model's modes of variability may be distinct from those found in nature, we have identified model and observed modes separately. All observed and modelled REOFs were calculated using data for the entire northern hemisphere north of 20^0N, and for the years 1970-1993; lack of data in the Pacific region made analysis of the observed fields in earlier years unreliable.

A 20 year daily climatology (1971-90) was calculated and then smoothed by taking the 5-day running mean. Daily anomalies from the smoothed climatology were calculated, and a low-pass 11 point non-recursive filter (Walraven 1984) applied to them to remove synoptic scale variations with periods of about eight days or less (i.e. anomalies of less than 4 days duration). The response of the filter is shown in fig.6. The filtered daily anomalies for the winter season (JFM) were then selected for further analysis. The filtered daily anomalies were sampled at 5 day intervals, and interpolated to an equal area grid, with a meridional resolution of 5^0, and zonal resolution equivalent to 10^0 at the equator. Correlation EOFS were calculated on this equal area grid, and the leading 15 EOFs rotated using the VARIMAX rotation algorithm. To display the REOFs, more easily done on the model grid, the correlation coefficients between the original filtered daily anomalies and the time coefficients of each REOF were calculated. It is the maps of these correlations which are shown in fig.7.

In calculating the model REOFs, daily 500 hPa data from a single run only were used, due to computational restrictions. However, the process was repeated for two further runs, and the modes discussed below were clearly identified among the leading modes in each case (spatial correlations greater than 0.9). As a further test on robustness, the analyses were repeated with the 5 day sampling starting from a different day, thus giving a different set of daily data. Again, little change was found in the major features of the leading modes.

Fig.7 shows the patterns which have the strongest weightings in the NPA sector.

Adjacent to each observed REOF is the corresponding model mode. As the REOFs were calculated using hemispheric data, the percentage of variance explained by each mode in the NPA sector was calculated from the correlations shown in fig.7 (using the area weighted average of their squared values). The values are listed in table 5. Calculated in this way the 4 modes shown in fig.7 between them explain about half of the variance in the NPA sector (45% for observed, 53% for model).

TABLE 5.

mode	% variance explained in NPA sector observed	model	Spatial Correlation model V observed in NPA sector
PNA	12.4	10.2	0.78
WP	11.6	15.1	0.62
EP	10.5	14.7	0.87
NP	10.2	12.9	0.88

The observed mode explaining the highest amount of variance in the NPA sector is shown in fig.7a. This is the well known Pacific North American (PNA) pattern described by Wallace and Gutzler (1981) in an analysis of monthly data, and by many subsequent authors. The PNA pattern has four anomaly centres which take alternate signs in the following order: Hawaii; the North Pacific; north-west America; and the south-eastern United States. The pattern is seen only in the cold half of the year (Barnston and Livezey 1987), but on a wide variety of time-scales from days and months through seasons to decades (Blackmon et al 1983/84). In fig.7a, the three extratropical centres of action are clear, showing the conventional 'positive' phase of the PNA pattern, i.e. with a strong negative centre over the North Pacific. The corresponding model mode is shown in fig.7b. Agreement between modelled and observed PNA modes is generally good (see table 5) but the model's North Pacific centre is less extensive and centred to the east of the corresponding observed node. Due to its more limited extent, the model PNA explains slightly less of the variance in the NPA sector than does the observed.

The second observed mode for the NPA sector, shown in fig.7c, is the West Pacific mode, WP. It corresponds to West Pacific modes identified in monthly 700 hPa height data by Horel and Wallace (1981), and Barnston and Livezey (1987). Its main feature is a north/south dipole in the western Pacific; a weaker north/south dipole of opposite polarity lies over the north American continent. The model simulates the western Pacific dipole well (fig. 7d), although the southern centre is located a little too far north. However, the model's pattern over America is quite different to that of the observed REOF, having a monopole centred over the Great Lakes; this reduces the spatial correlation between the modelled and observed modes (see table 5).

The third observed mode for the NPA sector, is an eastern Pacific pattern (EP), shown in fig.7e. The EP mode has a north/south dipole in the eastern Pacific, one node centred over Alaska, the other near Hawaii at around 30 S. A third node, in phase with that over Hawaii, lies over the Great Lakes. The corresponding model REOF pattern (fig.7f) agrees very well with the observed pattern (see table 5). The EP mode is very close to the 12th hemispheric REOF at 700 hPa seen in Richman (1994), and its two western centres closely resemble the East Pacific mode of Barnston and Livezey (1987), although the node over eastern Canada

is absent in their analysis.

The final observed mode for the NPA sector, shown in fig.7g, is the North Pacific pattern, NP. One centre is located over southern Japan, and this merges into a second centre of the same sign which lies to the west. A broader northern node of opposite phase lies above these two centres. The corresponding model mode (fig.7h) is in good agreement with the observed NP pattern (see table 5). The NP mode is very close to the 8th hemispheric REOF at 700 hPa seen in Richman (1994).

Considering all four REOFs shown in fig.7, the model shows a good level of agreement with the observed analyses. We therefore conclude that the modes of low-frequency variability of the NPA sector in winter (JFM) are well simulated by the model. We now wish to investigate how these modes of variability are influenced by SSTs, and in particular SSTs in the tropical Pacific.

b) Influence of SSTs on the leading winter NPA modes in model and observations

1) Influence of SSTs on the Pacific North American Mode in JFM

Interannual variations of the PNA mode (and other modes; see subsequent sub-sections) are investigated using a number of complementary approaches. First, we study the interannual time series by calculating seasonal (JFM) means of the filtered daily REOF amplitudes. These 'seasonal time-coefficients' are shown in Fig.8a for modelled and observed data; the latter were calculated only when spatial coverage was considered sufficient (from 1968). Fig.8a shows the individual model runs to be in good agreement: almost half their interannual variance can be explained by the common SST and sea-ice forcing (see table 6). Agreement with observations is also good: the modelled interannual evolution of the PNA mode is very well captured, given the degree of random variability (compare r_{EM} and $r_{EM.crit}$ in table 6).

TABLE 6. For seasonally averaged time-coefficients of each of the NPA modes: percentage of variance explained by oceanic forcing (ρ), and correlation (r_{EM}) between ensemble mean and observed values, together with the expected correlation for a 'perfect' model ($r_{EM.crit}$).

Mode	ρ (1949-93)	r_{EM} (1968-93)	$r_{EM.crit}$
PNA	46.5	0.66	0.67
WP	17.6	0.18	0.31
EP	7.8	0.05	0.16
NP	9.0	-0.26	0.18

In order to identify which areas of SST most influence the PNA mode, fig.8b (8c) shows correlations of GISST data versus observed (model ensemble mean) seasonal PNA time-coefficients. For consistency, both figures are based on data for 1968-93; use of model data over the full period of integration makes little difference. Note that for the calculation of significance, account was taken of serial correlation following Folland et al (1991). The model and observed patterns of correlation are very well matched, with similarly extensive areas of significant correlations. They differ significantly only over the central North Pacific, where the observed correlations are more strongly negative. Elsewhere model correlations tend

to be stronger than the observed, which is expected given higher signal-to-noise ratios of ensemble mean values. The link between the PNA mode and ENSO, highlighted in previous studies using monthly mean data (e.g. Horel and Wallace 1981, Yarnal and Diaz 1986), is clearly revealed in the pattern of correlations in figs.8b and 8c. One further point of interest is the strong correlations found in the extratropical North Pacific; positive along the coast of America, and negative in the central Pacific. Recent studies indicate that such SST anomalies are driven by the extratropical atmosphere (Frankignoul 1985, Alexander 1992), which thus links extratropical and tropical Pacific SSTs. If our model's PNA mode responds correctly to tropical Pacific SSTs, strong correlations with the prescribed extratropical Pacific SSTs will inevitably also be obtained (Graham et al 1994). The influence of extratropical SSTs on the atmosphere is thus hard to assess. However, there is evidence that this pattern of North Pacific SST anomalies may influence storm track positions, which in turn influence the anomalous large-scale flow, such that the likelihood of a PNA event is increased. A positive feedback between the extratropical atmosphere and ocean may thus be established (Trenberth and Hurrell 1994, Palmer 1988b,1993). Since, in our experiments, the pattern of SSTs is not produced by the model atmosphere, then such a feedback is not possible, and a relatively small error in the model, for example in storm track position or strength, could prevent the influence of extratropical SSTs from being properly simulated. This may account for the lower simulated correlations in the North Pacific compared with the observed (cf. Palmer 1995).

Cross-spectral analysis of modelled and observed seasonal PNA time-coefficients (see fig.9) reveals that they are significantly coherent on time-scales of approximately 2.5-8 years (significance at 95% level, calculated as in Bloomfield 1976). This frequency range matches that associated with ENSO. Filtering the PNA time-series to isolate this frequency band increases the percentage variance explained by SSTs to 58%, and the correlation between filtered ensemble mean and observed values to 0.78.

To give more insight into the relation between El-Nino type patterns of SST and the PNA pattern, the relative frequency of occurrence of the positive and negative PNA modes in warm and cold event years has been investigated. Using JFM data for all the years 1968-93, a probability distribution estimate (PDE) was calculated for the daily filtered PNA mode time-coefficients. Then, as in our composite calculations, the available years were ranked in order of the NINO3 SSTs, and data from the top and bottom quartiles pooled to give 'warm event' and 'cold event' subsets, for which PDEs were then calculated separately. Each PDE was calculated using a Gaussian kernel estimator which gives the PDE of a variable x as

$$P(x) = \frac{1}{N\alpha\,\sigma\,\sqrt{2\Pi}} \sum_{j=1}^{N} \exp\left[-(x-x_j)^2/2\,(\alpha\,\sigma)^2\right]$$

where x are the observed data, σ their standard deviation and N their number (Molteni et al 1990). α determines the level of smoothing, and was set to 0.3; this corresponds approximately to a histogram with 8 bins over $\pm 2\,\sigma$, however since the distributions are only used for display, the value of α is not critical.

The significance of the change in population between warm and cold event years can

be assessed by applying the standard Kolmogorov-Smirnov (KS) test (e.g. Hoel 1971, Press et al 1992) to the daily filtered time-coefficients, once the degrees of freedom have been adjusted to take account of the high serial correlation in the data. Using an F-test, the significance of differences in standard deviation between the warm and cold event subsets may also assessed, again with the reduced degrees of freedom. All results quoted below as significant pass the appropriate test at the 95% confidence level, unless explicitly stated otherwise.

PDEs for the observed PNA mode are shown in fig.8d. The 'all years' curve (solid line) is asymmetric: there are more high amplitude cases when the mode is negative, more small amplitude cases when it is positive. This implies greater variability in the negative PNA mode, consistent with the suggestion of Palmer (1988a and 1993) that the atmosphere is more barotropically stable when the PNA mode is in its positive phase. In warm event years (dotted line) the distribution shifts towards positive values, and the number of high amplitude negative cases is reduced. Conversely, in cold event years (dashed line) the number of negative cases increases, and the number of positive cases is markedly reduced. The KS test shows warm and cold event populations to be significantly different. In addition, the standard deviation of the filtered daily coefficients in warm event years is significantly less than that in cold event years, consistent with the greater variability of the negative phase.

The corresponding results for the model are shown in fig.8e. The modelled PNA time-coefficients essentially show the same behaviour as the observed; and the KS test shows warm and cold event distributions to be significantly different at a confidence level of 99%. The standard deviation of the filtered daily coefficients in warm event years is also significantly less than that in cold event years. Most previous studies have focused on the link between warm events and the positive phase of the PNA pattern, perhaps because links between cold events and the negative phase have proved rather more tenuous when investigated (e.g. Cubasch 1985). Our results show that cold events do have a strong influence on the PNA mode, such that negative PNA episodes predominate. However, the PNA response in cold event years could be more difficult to detect than that in warm events years, due to its greater variability.

The ENSO-induced changes in the frequency of occurrence of the opposing phases of the PNA mode are also clearly illustrated in fig.10. Here, the daily filtered time-coefficients of the PNA mode have been used to assess the duration of PNA episodes. The critical value for defining an episode was chosen as a time-coefficient of |1.25|. This includes (approximately) the highest 10% and lowest 10% of all time-coefficients from modelled and from observed analyses; from visual inspection these are associated with patterns that correspond reasonably well to the REOF modes. If the critical value is exceeded on n consecutive days then an episode of n days duration is said to have occurred. Filtered daily coefficients, rather than the unfiltered daily values, were used to assess duration. In general this makes little difference to the calculated duration of the PNA episodes, but in some cases it does prevent short timescale variations from breaking up what is clearly a single episode. The diagram shows distributions from observed and pooled model data. The observed distributions are more noisy, since they are based on less data, but are in generally good agreement with the modelled distributions. The occurrence of observed positive and negative PNA episodes is not governed solely by the phase of ENSO: one of the longest positive PNA episodes, of 23 days duration, occurred in a weak cold event year (1985). Nevertheless, the

influence of ENSO is clearly apparent in fig.10 with episodes tending to be longer and more frequent when the phase of ENSO is favourable. The longest observed episode, lasting 41 days, was a positive episode in 1983, the warmest of the warm events in the period studied. The model positive PNA episodes tend to be of shorter duration than the observed, the longest in 1983 was 16 days, perhaps because the model fails to respond correctly to extratropical SST patterns, or to errors in the stability of the model's basic flow. As we have few observed episodes, conclusions about the relative durations of positive and negative events are hard to draw; however the model shows a tendency for the negative events to be of longer duration. This is consistent with the observed results of Dole and Gordon (1983), and the ideas expressed by Palmer (1988a) that the negative PNA phase is more barotropically unstable, allowing the growth of perturbations with greater amplitude.

Although at a maximum on ENSO timescales, the coherence of model and observed PNA time series is still high on longer timescales (see fig.9). Fig.11a shows the ensemble mean (solid line) and the observed time series (dashed line) after filtering to remove fluctuations on timescales of less than 8 years. The filtered NINO3 SST time series is also shown (dotted line). All three time series show a shift towards positive values over the period 1977-87, although this is considerably less for the ensemble mean values (amplitude less than half that of the observed PNA time series). The period 1977-87 has often been referred to as one of climate shift in the North Pacific. The most striking change in this period was a deepening of the Aleutian low in the winter season, corresponding to a shift towards the positive phase of the PNA (though this was not seen in every year). Concurrent changes in surface winds, in sea-ice extent and ocean temperatures, and in temperature and precipitation over the U.S. were also observed (Trenberth and Hurrell 1994, UNESCO 1992). Analysing the model runs, we find that 54% of the variance in the filtered time series can be attributed to oceanic forcing. The corresponding expected correlation ($r_{EM,crit}$) between the ensemble mean and the observed filtered time series is 0.69; the actual correlation is slightly higher at 0.73. With the few degrees of freedom in the filtered data, this correlation is on the borderline of significance at the 95% confidence level. It is therefore difficult to claim that the model reproduces the observed decadal fluctuation. However, the decadal anomalies of modelled and observed surface temperature in the NPA sector shown in figs. 11b and 11c, show that the model does capture the pattern of anomalies well, although the anomalies are considerably weaker than the observed.

Further analysis reveals why the model did not pick up the strong average PNA state in 1977-87 with adequate amplitude. The model simulates the positive PNA response in warm event years (1977,1983,1987) well, but fails to capture the observed PNA response in the non-ENSO years (1978,1981,1984,1986) (see fig.8a). Taking the average of the JFM SSTs in these non-ENSO years reveals the only region with strong anomalies to be the North Pacific, where the east/west dipole pattern usually seen in conjunction with warm and cold events is apparent. As previously discussed, this pattern of SSTs is primarily the effect, rather than the cause, of the PNA pattern. So, on the one hand, the strong PNA response in non ENSO years may be unrelated to direct SST forcing, and solely the result of random variation in the extratropical atmosphere. However, the strength of the observed PNA index in these non-ENSO years is unusual, outside the range of the ensemble spread, and this may alternatively be partly due to a possible failure of the model to respond correctly to the prescribed extratropical SSTs, as discussed above.

2) Influence of SSTs on the West Pacific mode in JFM

In fig.12a the model and observed seasonal time coefficients of the WP mode are shown. The poor agreement between the different model runs indicates that the SST forcing has little influence on the model mode, and the correlation between the ensemble mean and the observed time-coefficients is correspondingly low, less than expected (but not significantly so) given the level of variance explained (see table 6). Cross-spectral analysis fails to reveal any timescale on which the observed and modelled JFM WP modes are significantly coherent.

Figs. 12b,12c show correlations of GISST data with the seasonal WP time-coefficients using observed and ensemble mean values respectively. Had the model's WP pattern been responding to tropical Pacific SSTs correctly, then its correlations with GISST would have been generally stronger than the observed, as for the PNA mode, due to the higher signal-to-noise ratio of ensemble mean values. Instead we find the model correlations to be weaker and generally insignificant, while there is a distinct El Nino-like pattern of strong, significant correlations in the observed analysis.

Fig. 12d shows PDEs of the observed filtered daily WP time-coefficients in warm event, cold event, and all years, calculated as for the PNA mode. There is a shift towards the positive WP phase in warm event years, and a rather smaller shift toward the negative phase in cold event years. The KS test shows that the observed warm and cold event distributions are significantly different at the 99% confidence level. The corresponding distributions for the model coefficients, fig.12e, show PDEs in warm event and cold event years to be very similar: their difference is not significant.

In summary, the model simulates the spatial pattern of the WP mode generally well, although it does differ from the observed mode over the American continent. However, the model mode shows no significant dependence on tropical Pacific SSTs, and little dependence on SSTs in general, while the observed WP mode is strongly influenced by tropical Pacific SSTs. Not surprisingly therefore, the interannual evolution of the observed and modelled modes are poorly correlated. The link between warm events and the positive phase of the WP mode in nature has been identified in earlier studies such as Livezey and Mo (1987), and Horel and Wallace (1981). As discussed by Hoerling et al (1992), the extratropical response to ENSO is sensitive to errors in the model climatology. It appears that in our model there is some error in the chain that should couple tropical Pacific SSTs and extratropical anomalies in the western Pacific. Such an error would also explain the discrepancies between model and nature seen in our composites over the north-west Pacific (figs.2 and 3).

3) Influence of SSTs on the East Pacific Mode in JFM

In fig.13a the seasonally averaged time-coefficients of the EP mode are shown. Agreement between different model runs is poor, and agreement between ensemble mean and observed EP time-coefficients is correspondingly low (table 6), indicating interannual variations of this pattern are probably random. Cross spectral analysis reveals no time scale on which observed and modelled time series are significantly coherent.

Correlating the EP time-coefficients with the GISST data set, reveals few significant values, as seen in figs. 13b and 13c. The strongest correlations of the observed analysis are

with SSTs in the North Atlantic. This banded pattern of correlations is a well known mode of Atlantic SSTs (Lau and Nath 1990, Kushnir 1994), usually associated with the North Atlantic Oscillation (e.g. Davies et al 1996). Model correlations form a similar pattern in this North Atlantic region, but are rather weaker, significantly so to the south of Greenland. Over the rest of the world's oceans there are few areas of significant difference between the two correlation maps. Figs. 13d and 13e show the PDEs for the observed and modelled modes respectively, there is good agreement between their 'all year' PDEs : both are skewed toward small negative values, and have more high amplitude positive cases. The PDEs for warm event years differ little from those for cold event years for model values, and although there appears to be a larger shift for observed values, KS tests indicate that the difference is not significant at the 95% level.

In summary, the impact of SSTs on the EP mode is negligible. In particular tropical Pacific SSTs do not have a discernable influence. There is some suggestion of a link with Atlantic SSTs, particularly in the observed data, but the question of cause and effect has not been addressed. The model gives a good simulation both of the EP pattern, and of its independence of tropical Pacific SSTs.

4) Influence of SSTs on the North Pacific Mode in JFM

Fig.14a shows the seasonal time-coefficients of the NP mode. Again there is little agreement between model runs, and correlation between the ensemble mean and the observed time-coefficients is not significantly different from zero (see table 6). Cross-spectral analysis reveals no time scales on which observed and modelled time series are significantly coherent.

Fig.14b shows correlations between GISST data and the observed seasonal NP time-coefficients. There are some relatively high correlations in the North Pacific, approximately coincident with the NP nodes. Such correlations may reflect the influence of the mode on the SSTs in addition to, or instead of, the reverse influence. In the tropics, the correlations follow an El Nino pattern, although only a few areas are significant. The model correlations (fig. 14c) show little correspondence to the observed, and few areas of significance. The observed PDEs (fig.14d) show a preference for the positive NP phase in warm event years, and a corresponding shift to the negative phase in cold event years; the KS test indicates that the two sets of time coefficients are significantly different at the 99% level. Looking at the number of NP episodes of different durations (not shown), confirms the influence of ENSO on the observed NP mode. Neither the model correlation map, shown in fig.14c, nor its PDEs, shown in fig.14e, reveal any dependence of the model's NP mode on tropical Pacific SSTs.

Although the model and observed NP EOFS are in very good agreement, the former is little influenced by SSTs, while the latter is clearly subject to influence by tropical Pacific SSTs. It seems then that the model, perhaps due to failure in simulating the atmospheric response in the western tropical Pacific, does not reproduce the observed modulation of the NP mode.

5. Summary and Conclusions

We have studied an ensemble of six 45-year runs of the Hadley Centre's HADAM1 atmospheric climate model. The runs are for the period 1949-93, and are forced with observed sea-ice and SSTs from the GISST1 data set. Our focus has been the response to ENSO in the model atmosphere, in particular that in the North Pacific American (NPA) sector.

The seasonal composites of MSLP, surface air temperature and precipitation, discussed in section 3, show that the atmospheric response to ENSO is reasonably well simulated throughout the globe, with interannual variations of the SOI being particularly well captured. The model composites, with their amplified signal-to-noise ratio, also serve to highlight weak ENSO responses, which may be difficult to detect in the observed record. Examples of such responses include: the MSLP signal over the North Atlantic in DJF, corresponding to increased blocking in warm event years; cooling over New Zealand in DJF, and in Japan and Canada in JJA in warm event years (and warming in cold event years); and most of the precipitation signals discussed in section 3e. From the seasonal composite analysis, we find the pattern of anomalies in the opposing phases of ENSO to be approximately inverse over much of the globe in both model and observations. This suggests an approximately linear response to ENSO, although there is considerable variability in response from one warm (or cold) event to another. Composites for the NPA sector in the season JFM show that the model and observed atmospheres respond similarly to ENSO, although the modelled anomaly centres in the North Pacific are off-set from the observed.

In section 4a, we show that the leading JFM modes of variability in the NPA sector are well simulated by the HADAM1 model. The modes were identified on their natural timescales by analysing daily 500hPa height data, low pass filtered to remove synoptic timescale variations. Four leading modes were identified for the NPA sector: the Pacific North American (PNA), West Pacific (WP), East Pacific (EP) and North Pacific (NP). In section 4b, a correlation analysis of SST with the mode's seasonally averaged (JFM) time-coefficients revealed a strong influence of ENSO on three of the observed modes (PNA, WP and NP). This was confirmed by analysis of the daily filtered REOF time-coefficients: significant shifts are seen in the distributions of the PNA, WP and NP time-coefficients on moving between warm and cold event years. The model fails to reproduce the influence of ENSO on the WP and EP modes, but the influence of warm and cold events on the PNA mode is captured very well. With analysis of variance techniques we can quantify the strength of the influence of SSTs on the model's PNA mode: almost half of the variance of the seasonal means is attributable to the oceanic forcing (47%). We also find that, given the limits due to random variation, the temporal evolution of the modelled and observed PNA patterns are in excellent agreement. Since ENSO has a more consistent effect on the PNA mode than on the other modes identified, the seasonal ENSO composites look most like this pattern in the NPA sector, except in the north-western Pacific where the WP and NP modes also have some impact. The differences between modelled and observed seasonal composites, shown in section 3, therefore largely reflect the differences between modelled and observed PNA modes.

In nature there was a clear preference for the positive phase of the PNA over the period 1977-87, which resulted in strong decadal anomalies in the NPA sector, very similar to warm event composite anomalies. The years 1977-87 include three strong warm events, and

only one counteracting weak cold event, thus biasing the decadal average toward the positive phase of the PNA; but the non-ENSO years of this period also make a strong contribution to the observed decadal anomalies. The model response over the same period reproduces the *pattern* of decadal anomalies well, corresponding to the positive phase of the PNA, but with a *magnitude* that is much to weak. This is because while capturing the PNA response in warm event years, it fails to do so in the non-ENSO years. The differences in model and observed PNA response in non-ENSO years can largely be attributed to the internal variability of the atmosphere, although it is possible that a failure by the model to respond correctly to extratropical SST anomalies could also have some effect. The decadal anomalies in the North Pacific demonstrate that long timescale variations in modes such as the PNA can have large impacts on regional temperatures. The ability to simulate and understand such variations is important for studies of anthropogenic climate change. In future such decadal variations will be studied in 125 year-long integrations forced with observed SSTs, which are currently under way at the Hadley Centre.

The strong relationship between ENSO and weather patterns in the NPA sector make useful seasonal forecasts for this region viable in the winter half year (e.g. Livezey 1990). Davies et al (1996) have shown that the model discussed here is also skilful in simulating the leading modes of variability in the North Atlantic / European (NAE) sector. In future we also intend to analyze these NAE modes of variability on their natural timescales in terms of the distribution of time-coefficients, using the techniques described in this paper. This will help in understanding both the prospects for seasonal forecasting in this region, and the long timescale variations of modes such as the North Atlantic Oscillation, and its impact on climate.

Acknowledgements. Thanks are due J.Davies and D.Sexton for helping to run the model integrations. Observed MSLP data were kindly provided by T.Basnett and D.E.Parker, and D.P.Cullum provided the air temperature data. Gridded observed rainfall data (GU23WLD0094.DAT) was constructed by Mike Hulme at the Climate Research Unit, Norwich, under DoE contract PECD7/12/78, and Tahiti and Darwin MSLP data were supplied by Phil Jones. This work was carried out under the UK Department of Environment contract PECD/7/12/37, with further partial support under CEC contract no EVSV-CT92_0121 ("Medium Term Climate Variability")

REFERENCES

Alexander,M.A., 1992: Midlatitude atmosphere-ocean interaction during El Nino. Part I. The North Pacific Ocean. Part II the Northern Hemisphere atmosphere. *J.Climate*, **5**, 944-972

Barnston, A.G., and R.E.Livezey, 1987: Classification and persistence of low frequency atmospheric circulation patterns. *Mon. Wea. Rev.*, **115**, 1083-1123.

Barnston,A.G., 1994: Linear statistical short-term climate predictive skill in the northern hemisphere. *J.Climate*, **7**, 1513-1564.

Barnston,A.G., 1995: Our improving capability in ENSO forecasting. *Weather*, **50**, 419-430.

Barnett,T.P., 1988: Variations in near global sea level pressure: another view. *J.Climate*, **1**, 225-230.

Barnett,T.P., 1994: Forecasting global ENSO-related climate anomalies. *Tellus*, **46A**, 381-397.

Basnett, T.A., and D.E.Parker, 1995: Provisional new global mean sea level pressure data set. In: "Workshop on Simulations of the Climate of the Twentieth Century using GISST, 28-30 November 1994, Hadley Centre, Bracknell, UK", Folland, C.K. and Rowell, D.P. (Eds), Climate Research Technical Note No.56 Workshop report, 58-59.

Bjerknes, J., 1969: Atmospheric teleconnections from the equatorial Pacific. *Mon. Wea. Rev.* **97**, 163-172.

Blackmon,M.L., J.E.Giesler, and E.J.Pitcher, 1983: A general circulation study of January climate anomaly patterns associated with interannual variation of equatorial Pacific SSTs. *J.Atmos.Sci*, **40**, 1410-1425.

Bloomfield,P., 1976: Fourier analysis of time series: an introduction. John Wiley and sons, pp258.

Bottomley, M., C.K.Folland, J.Hsiung, R.E Newell, and D.E.Parker, 1990: Global Ocean Surface Temperature Atlas. Joint Met. Office/MIT Project, 20pp. + 313 plates, funded by UK Depts. of Energy and Environment, HMSO, London.

Chen,W.Y., 1982: Fluctuations in northern hemisphere 700mb height fields associated with the southern oscillation. *Mon.Wea.Rev.* **110**, 808-823.

Cheng,X. ,G.Nitsche,and J.M.Wallace, 1995: Robustness of low-frequency circulation patterns derived from EOF and rotated EOF analyses. *J.Climate*, **8**, 1709-1713.

Chervin,R.M., 1986:Interannual variability and seasonal climate predictability. *J.Atmos.Sci*, **43**, 233-251.

Cubasch,U., 1985: The mean response of the ECMWF global model to the composite El Nino anomaly in the extended range prediction experiments. Pp 329-344 in coupled Ocean atmosphere models, ed J.Nihoul, Elsevier Press.

Davies,J.R., D.P. Rowell, and C.K.Folland, 1996: North Atlantic European seasonal Predictability using an ensemble of multi-decadal AGCM simulations. submitted to *Int.J.Climatol.*

Dole, R.M. and N.D. Gordon, 1983: Persistent anomalies of the extratropical northern hemisphere wintertime circulation: geographical distribution and regional persistence characteristics. *Mon. Wea. Rev.*, **111**, 1567-1586.

Folland,C.K., J.A.Owen, M.N.Ward, A.W.Colman, 1991: Prediction of seasonal rainfall in the Sahel region using empirical and dynamical methods. *J.Forecasting*, **10**, 21-56.

Fraedrich,K and K.Muller, 1992:Climate anomalies in europe associated with ENSO extremes. *Int. J. Climatol.*, **12**, 25-31.

Frankingnoul,C.J. , 1985: Sea surface temperature anomalies, planetary waves and air-sea feedback in the middle latitudes. *Revs. Geophys*, **23**, 357-390

Graham,N.E., T.P.Barnett, R.Wilde, M.Ponater, and S.Schubert, 1994:On the roles of tropical and Midlatitude SSTs in forcing Interannual to Interdecadal Variability in the winter Northern hemisphere circulation. *J.Climate*, **7**, 1416-1441.

Halpert,S.H. and C.F.Ropelewski, 1992: Surface temperature Patterns associated with the southern oscillation. *J.Climate*, **5**, 57-593.

Held,I.M. , S.W.Lyons, and S.Nigam, 1989: Transients and the extratropical response to ENSO. *J.Atmos.Sci* **46**, 163-174

Hildebrandsson, H.H., 1897: Quelques recherches sur les centres d'action de l'atmosphere. Svenska Vet. Akad. Handlingar.

Hoel, P.G., 1971: Introduction to mathematical statistics. John Wiley, New York, 409pp

Hoerling,M.P., M.L.Blackmon, and M.Ting, 1992: Simulating the Atmospheric response to the 1985-87 El Nino cycle. *J.Climate*, **5**, 669-682.

Hoerling,M.P., and M.Ting, 1994: Organization of extratropical transients during El Nino. J.Climate,7,745-766.

Horel,J.D. and J.M.Wallace, 1981:Planetary Scale phenomenon associated with the Southern Oscillation. *Mon. Wea. Rev.* **109**, 813-829.

Hoskins,B.J. and D.J.Karoly, 1981: The steady linear response of a spherical atmosphere to thermal and orographic forcing. *J.Atmos.Sci*, **38**, 1179-1196.

Hulme,M., 1994: Validation of large scale precipitation fields in general circulation models. In:'Global Precipitation and climate change, Debois,M and Desalmaud,F. (Eds.) NATO AS1 Series, Vol I 26, Springer-Verlag, Berlin, 387-405.

Jackson,M. 1986: Operational Superfiles in Met O 13. Met O13 Technical note 25 (available from the Hadley Centre, U.K.Met Office)

Jones,P.D., 1994: Hemispheric surface air temperature variations: a reanalysis and an update to 1995. *J.Climate*, **7**, 1794-1802.

Karoly,D.J., 1989: Southern Hemisphere circulation features associated with El Nino-southern oscillation events. *J.Climate*, **2**,1239-1252

Kiladis,N.K. and H.F.Diaz, 1989: Global Climatic anomalies associated with extremes in the southern oscillation. *J.Climate*, **2**, 1069-1090.

Konig,W, E.Kirk and R.Sausen, 1990: Sensitivity of an atmospheric general circulation model to interannually varying SST. A*nnales Geophysicae*, **8**, 829-844

Kushnir,Y., 1994: Interdecadal variations in the North Atlantic sea surface temperature and associated atmospheric conditions. *J.Climate*, **7**, 141-157.

Latif,M., J.Biercamp, H.von Storch, M.J.McPhaden and E.Kirk, 1990: Simulation of ENSO related Surface Wind Anomalies with an atmospheric GCM forced by observed SST. *J.Climate*, **3**, 509-521.

Lau,N.C., 1981: A diagnostic study of recurrent meteorological anomalies appearing in a 15 year simulation with a GFDL general circulation model. *Mon.Wea.Rev.*, **109**, 2287-2311.

Lau,N.C., 1985: Modelling the seasonal dependence of the atmospheric response to Observed El Ninos in 1962-76. *Mon.Wea.Rev.*, **113**, 1970-1996.

Lau,N.C., 1988: Variability of the baroclinic and barotropic transient eddy forcing associated with monthly changes in midlatitiude storm tracks. *J.Atmos.Sci*, **45**, 2718-2743.

Lau,N.C. and M.J.Nath, 1990: A general circulation Model Study of the Atmospheric response to Extratropical SST anomalies Observed in 1950-79. *J.Climate*, **3**, 990-998.

Lau,N.C. and M.J.Nath, 1994: A modelling study of the relative roles of tropical and extratropical SST anomalies in the variability of the global atmosphere-ocean system. *J.Climate*, **7**, 1184-1207.

Leathers,D.J., B.Yarnal, and M.A.Palecki, 1991:' The Pacific North American teleconnection pattern and United

States climate. part 1. Regional temperature and precipitation associations', J.Climate,4,517-528.
Livezey,R.E. 1990: Variability of skill of long-range forecasts and implications for their use and value. *Bull. A.M.S.*, **71**, 300-309.

Livezey,R.E. and K.C. Mo, 1987: Tropical extratropical teleconnections during the northern hemisphere winter. Part II: Relations between monthly mean northern hemisphere circulation patterns and proxies for tropical convection. *Mon.Wea.Rev.*, **115**, 3115-2004.

Livezey,R.E., C.K.Folland, J.Davies, D.Karoly, J.Walsh, M.Sugi, P.Gleckler and D.E. Parker, 1995: AGCM intercomparison diagnostics: Key time series. In: "Workshop on Simulations of the Climate of the Twentieth Century using GISST, 28-30 November 1994, Hadley Centre, Bracknell, UK", Folland, C.K. and Rowell, D.P. (Eds), Climate Research Technical Note No.56 Workshop report, 5-10.

Lorenz,E.N., 1963: Deterministic nonperiodic flow. *J.Atmos.Sci*, **20**, 130-141.

Molteni,F., S.Tibaldi and T.N.Palmer, 1990: Regimes in the wintertime circulation over northern extratropics. I) Observational evidence, II) Consequences for dynamical predictability. *QJRMet Soc*, **116**, 31-67.

Palmer,T.N.1995: The influence of north-west Atlantic sea surface temperature: An unplanned experiment. *Weather*, **50**, 413-419.

Palmer,T.N., 1993: Extended range atmospheric prediction and the Lorenz model. *Bull.Am.Met Soc.*, **74**, 49-65.

Palmer,T.N.1988 a: Medium and extended range predictability and stability of the Pacific North American mode. *Q.J.R.Met Soc*, **114**, 691-714.

Palmer.T.N.1988 b: Large scale tropical-extratropical interactions on timescales of a few days to a season. *Aust.Met.Mag*, 36, 107-125.

Pan,Y.H and A.H. Oort, 1983 : Global climate variations connected with Sea surface temperature anomalies in the eastern equatorial Pacific ocean for the 1958-73 period. *Mon. Wea. Rev*, **111**, 1244-1258.

Parker,D.E. , C.K.Folland, and M.Jackson, 1995: Marine surface temperature: observed variations and data requirements. *Climate Change*, **31**, 559-600.

Parker,D.E. , C.K.Folland, A.C.Bevan, N.M.Ward, M.Jackson, and K.Maksell 1996: Marine surface data for analysis of climatic fluctuations on interannual to century timescales. In: "Natural Climate variability on decade-to-century timescales", eds: D.G.Martinson, K.Bryan, M.Ghil, N.M.Hall, T.R.Karl, E.S.Sarachik, S.Sorooshian and L.D.Talley. National Acad. Press, Washington D.C., pp241-250. Colour figs pp222-228.

Phillips, T.J., 1994: A summary documentation of the AMIP models. PCMDI Report No.18, Univ. of Calif., Lawrence Livermore National Laboratory, Calif.

Press, W.H., S.A.Teukolsky, W.T.Vetterling, and B.P.Flannery, 1992: Numerical recipes in FORTRAN.

Cambridge University Press, 963pp

Richman,M.B. 1994: On the use of multivariate statistics to validate Global climate models. PhD Thesis, University of Illinois, 321 pp

Ropelewski, C.F. and M.S.Halpert, 1986: North American Precipitation and Temperature Patterns associated with the El Nino/Southern Oscillation. *Mon. Wea. Rev.*, **114**, 2352-2362.

Ropelewski, C.F. and M.S.Halpert, 1987: Global and regional scale precipitation patterns associated with the El Nino/Southern Oscillation. *Mon. Wea. Rev.*, **115**, 1606-1625.

Ropelewski, C.F. and M.S.Halpert, 1989: Precipitation patterns associated with the high index phase of the southern oscillation. *J. Climate*, **2**, 268-284.

Ropelewski, C.F. and P.D.Jones, 1987: An extension of the Tahiti-Darwin Southern Oscillation index. *Mon. Wea. Rev.*, **115**, 2161-2165.

Rogers,J.C.,1984: The association between the North Atlantic Oscillation and the Southern Oscillation in the Northern Hemisphere. *Mon.Wea.Rev*, **112**, 1999-2015.

Rowell,D.P, C.K.Folland, K.Maskell, and N.M.Ward, 1995: Variability of summer rainfall over tropical North Africa (1906-92): Observations and Modelling. *Q.J.R.Met. Soc.*, **121**, 669-704.

Rowell,D.P, 1996: Using an ensemble of multi-decadal GCM simulations to assess potential seasonal predictability. Climate Res. Tech. Note No. 69 (available from the Hadley Centre, U.K.Met Office) and in preparation for *J.Climate*.

Rowntree,P.R., 1972: The influence of tropical east Pacific ocean temperatures on the atmosphere. *Q.J.R.Met. Soc.*, **98**, 607-625.

Sardeshmukh,P.D. and B.J.Hoskins, 1988: The generation of global rotational flow by steady idealized tropical divergence. *J.Atmos.Sci*, **40**, 1613-1630.

Shukla,J and J.M. Wallace, 1983: Numerical simulation of the atmospheric response to equatorial Pacific sea surface temperature anomalies. *J.Atmos. Sci.*, **40**, 1613-1630.

Smith,I.N.1995: A GCM Simulation of Global Climate Interannual variability 1950-1988. *J.Climate*, **8**, 709-718.

Trenberth,K.E. and J.W.Hurrel, 1994: Decadal atmosphere-ocean variations in the Pacific. *Clim. Dynamics*, **9**, 303-319.

UNESCO, 1992: Oceanic interdecadal variability. IOC Technical Series 40 pp40.

Van Loon,H., 1986: The characteristics of sea level pressure and sea surface temperature during the development

of a warm event in the southern oscillation. Namias symposium, Scripps institute of oceanography,160-173.

Walker,G.T., 1924: Correlation in seasonal variations of weather, IX: A further study of world weather. *Memoirs of the Indian Meteorological Department*, **24**, 275-232.

Wallace,J.M. and D.S.Gutzler, 1981: Teleconnections in the geopotential height field during the northern Hemisphere winter. *Mon. Wea. Rev.*, **109**, 784-812.

Walraven,R., 1984: Digital filters, in: Proceedings of the digital equipment users society, Anaheim,California,Dec 1984 (unpublished document available from the department of Applied Science, University of California,Davis,California) 23-30.

Warrilow, D.A., A.B.Sangster, and A.Slingo, 1986: Modelling of land surface processes and their influence on European climate. Dyn. Climatol. Tech. Note No. 38 (unpublished document available from the Hadley Centre, UK Meteorological Office, Bracknell).

Willmot,C.J., C.M.Rowe, and Y.Mintz, 1985: A global archive of land cover and sils data for use in general circulation climate models. *J.Climatol.*, **5**, 119-143.

WMO, 1966:'Climate change',WMO technical note 79.

Yarnal,B. and H.F.Diaz, 1986: Relationships between extremes of the southern oscillation and the winter climate of the Anglo-American Pacific coast. *J.Climatol.*, **6**, 197-219.

F.W.Zwiers and H. von Storch: Taking serial correlation into account in tests of the mean. *J.Climate*, **8**, 336-351.

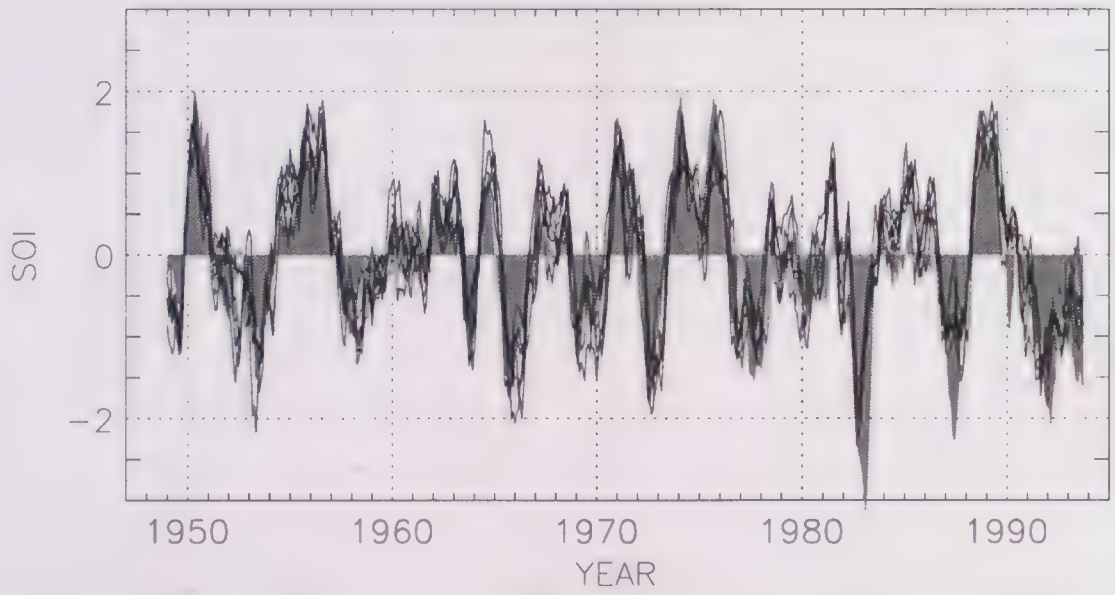

FIG. 1 Modelled and observed SOI, 1949-93. The SOI is calculated as the Tahiti minus Darwin difference in 5 month running mean values of normalized MSLP anomalies. Each solid line shows the SOI of an individual model integration. Grey shading shows the observed SOI.

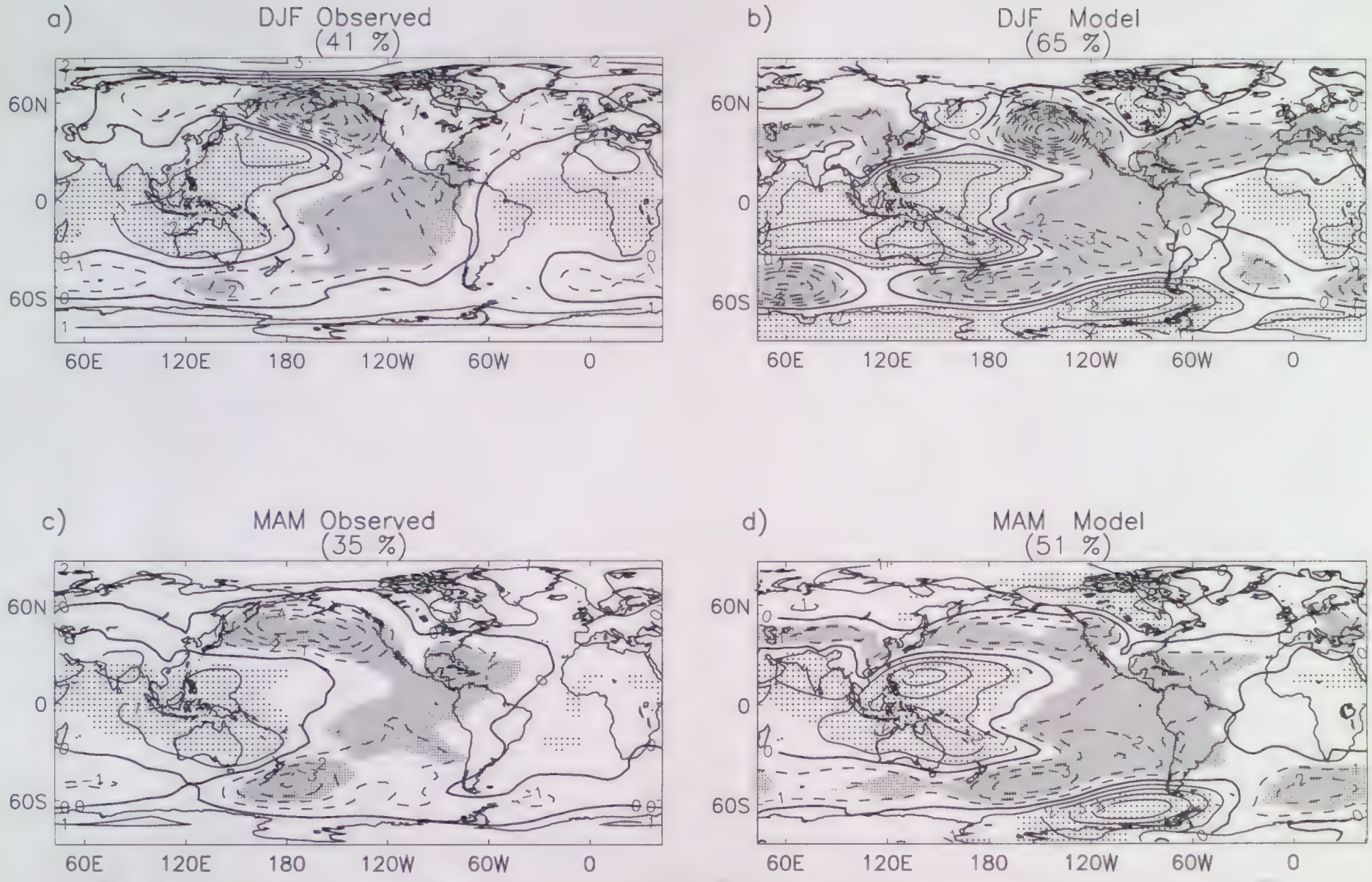

FIG. 2 Warm event (El Nino) minus cold event (La Nina) composite differences of MSLP, for the four standard seasons. Positive differences have solid contours, negative differences are dashed. Areas of significant difference (at the 95% level) are shaded.

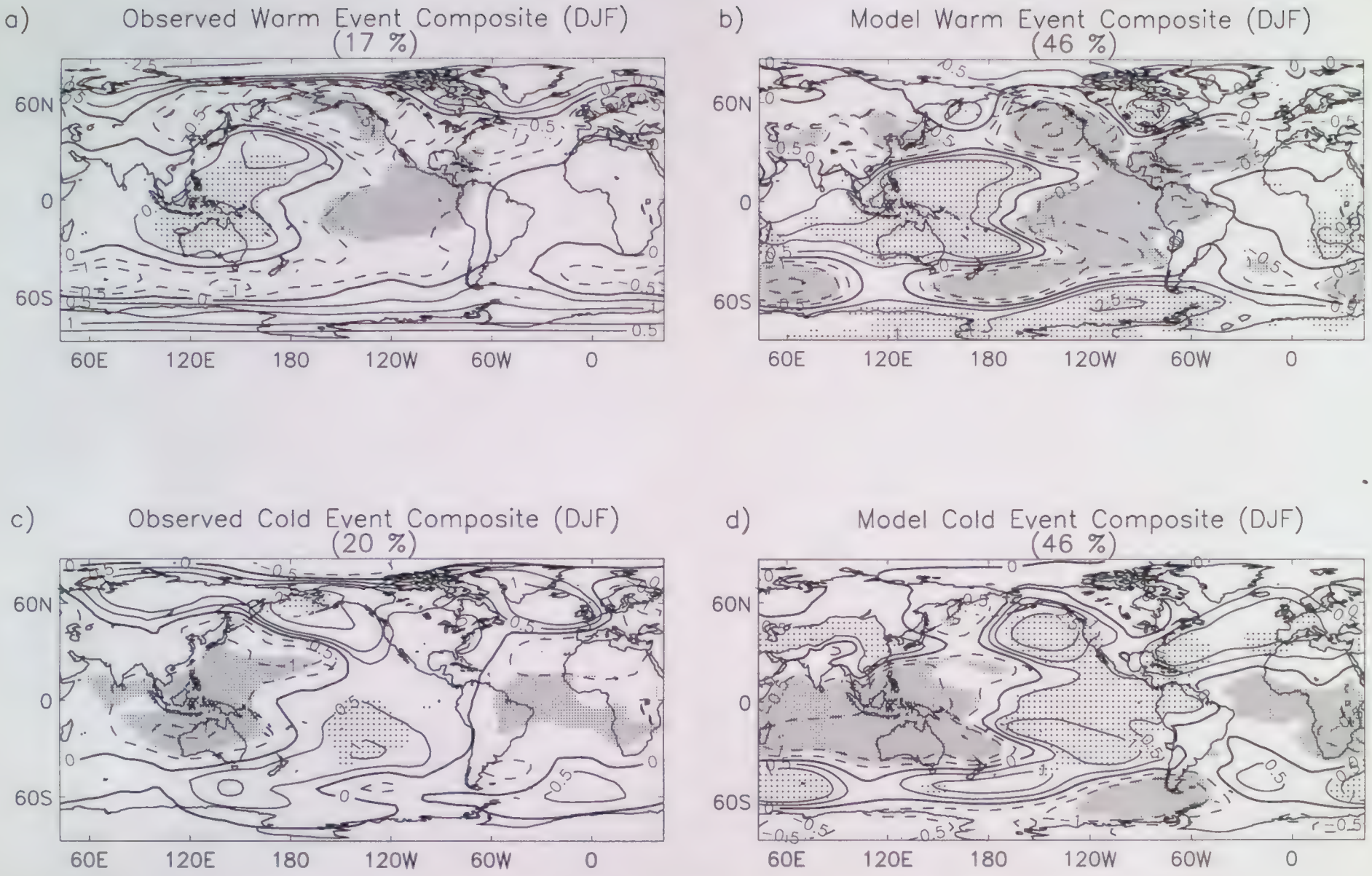

FIG. 3 Composite MSLP anomalies, wrt 1949-93 mean values, for DJF. Positive anomalies have solid contours, negative anomalies are dashed. Areas of significance (at the 95% level) are shaded.
a) warm event (El Nino) observed composite **b)** warm event (El Nino) model composite
c) cold event (La Nina) observed composite **d)** cold event (La Nina) model composite

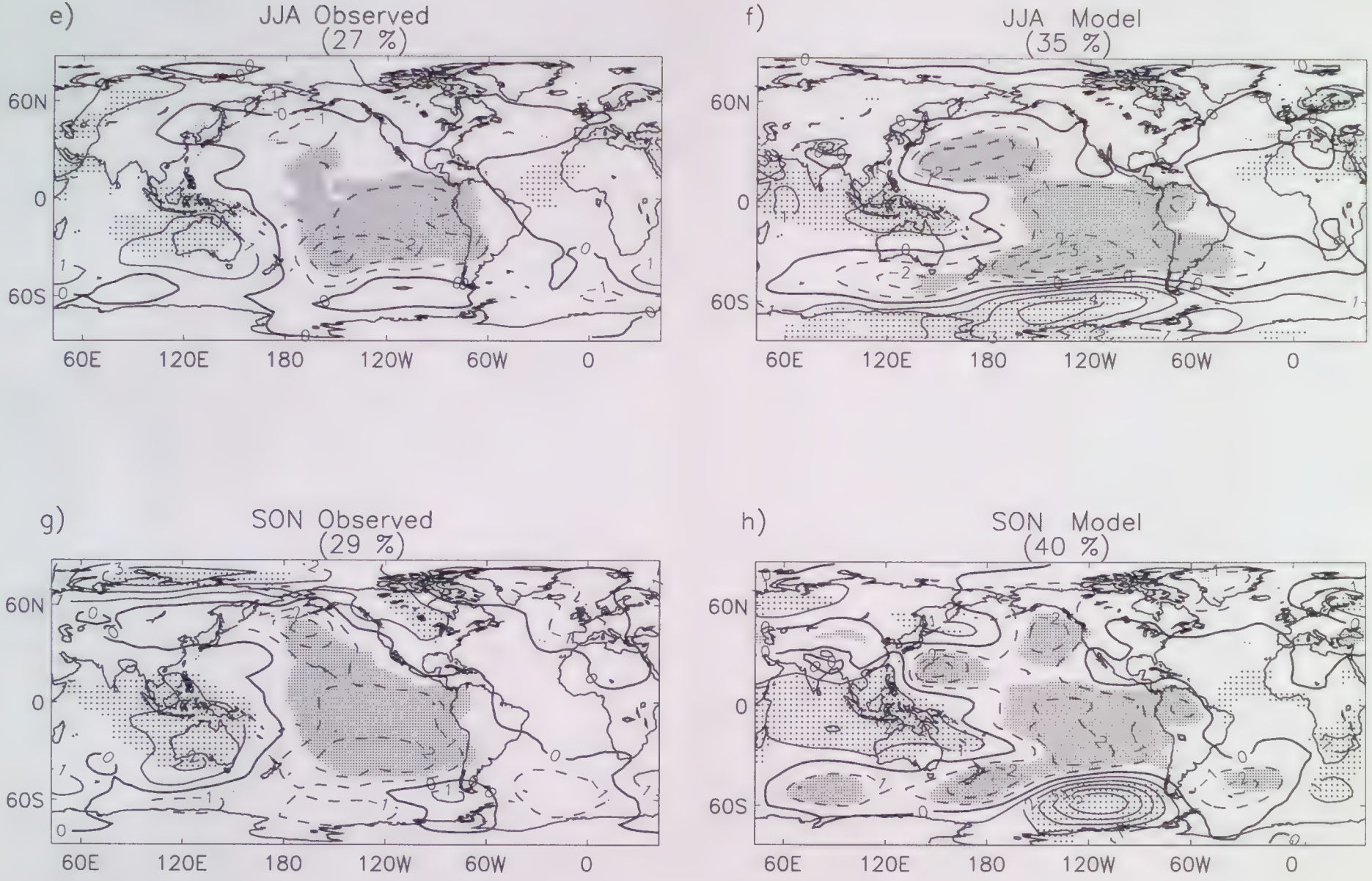
e)
JJA Observed
(27 %)
f)
JJA Model
(35 %)
g)
SON Observed
(29 %)
h)
SON Model
(40 %)
60N
0
60S
60E
120E
180
120W
60W
0

FIG. 2

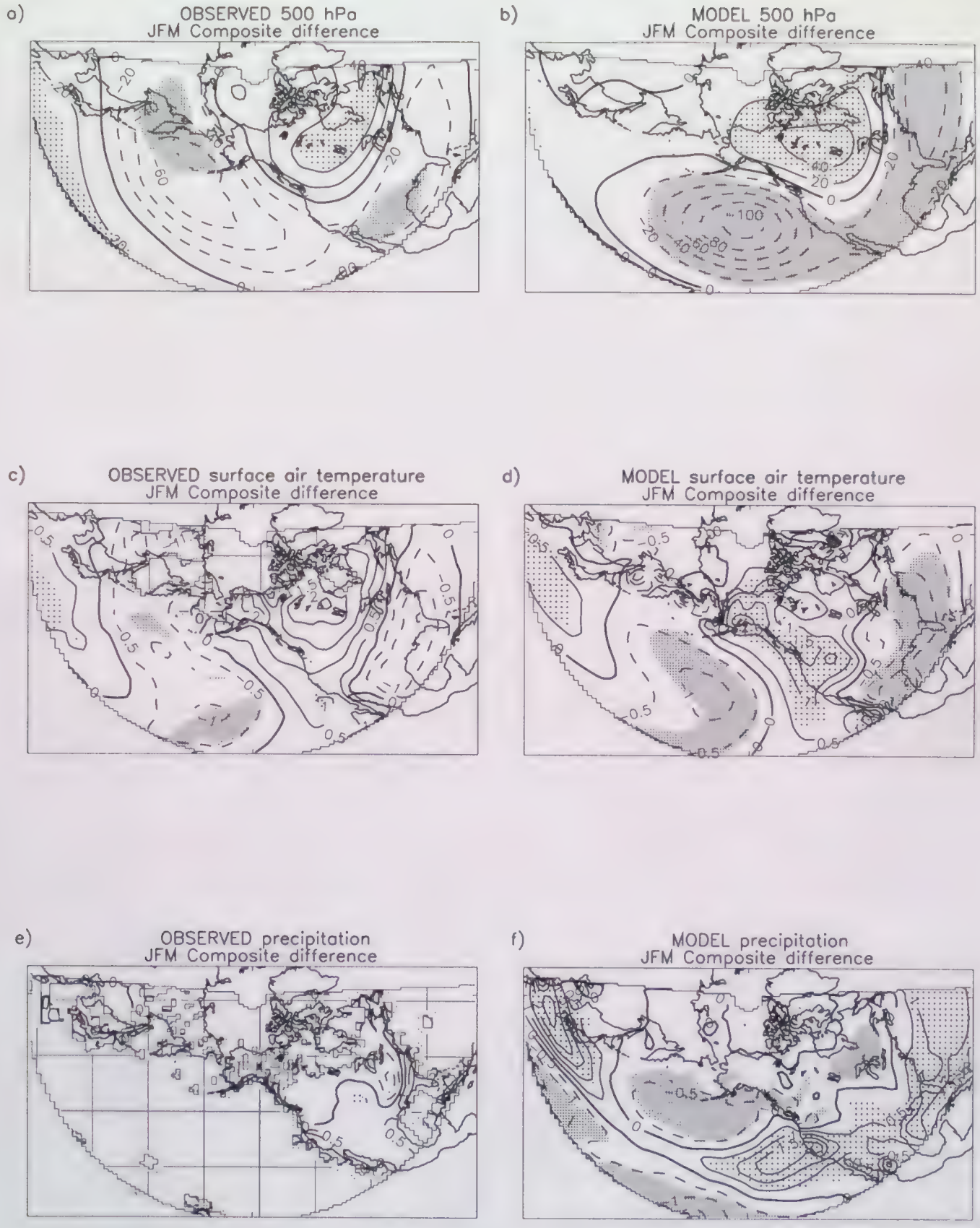

FIG. 4 a) Observed and **b)** Modelled warm event (El Nino) minus cold event (La Nina) composite differences of 500 hPa height, for the winter season JFM in the North Pacific American sector. Positive anomalies have solid contours, negative anomalies are dashed. Areas of significant difference (at the 95% level) are shaded. Cross-hatching indicates missing data.

c) and **d)** as a) and b) but for surface air temperature.

e) and **f)** as a) and b) but for precipitation.

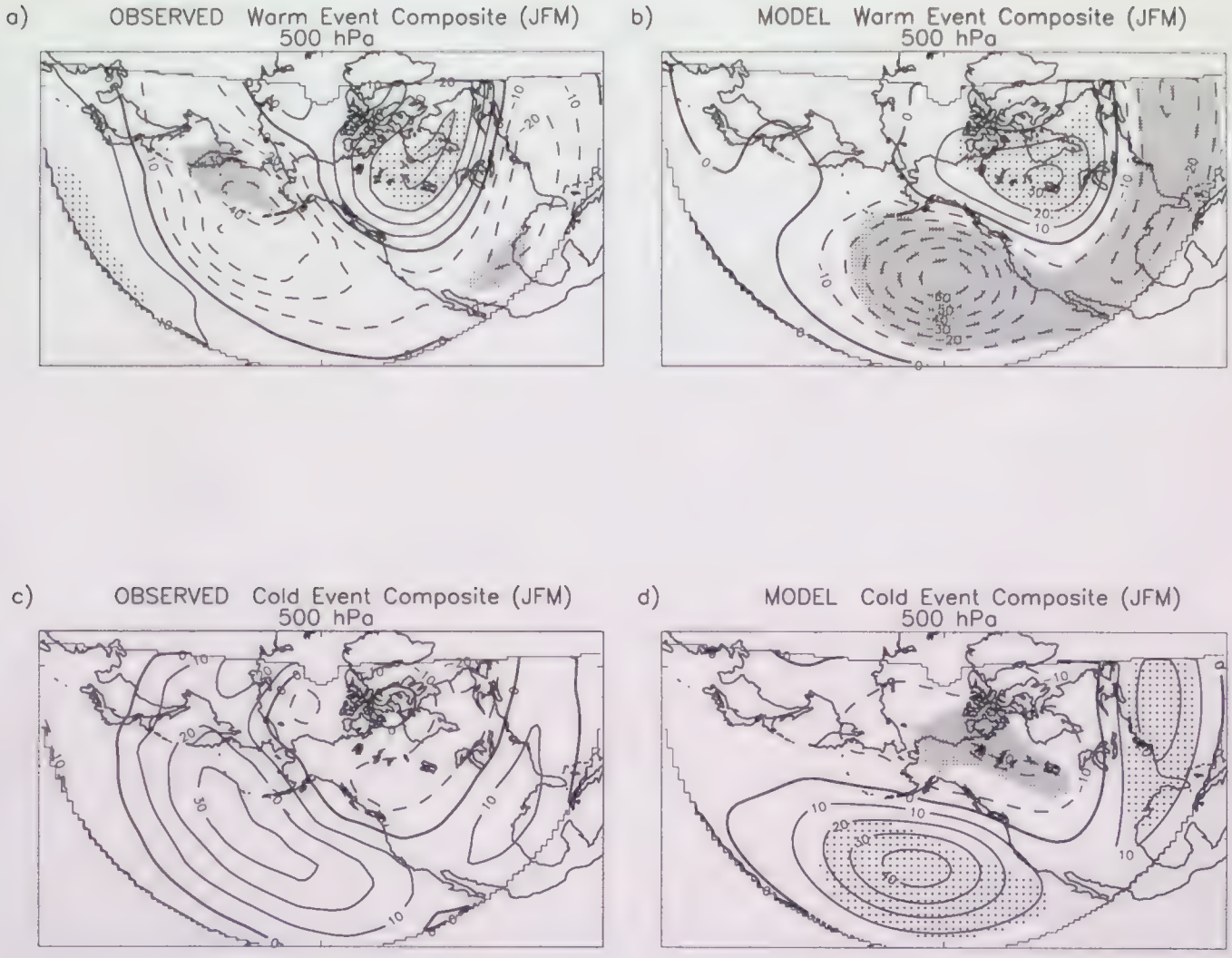

FIG. 5 Composite 500 hPa height anomalies, wrt 1949-93 mean values, for the winter season JFM in the North Pacific American sector. Positive anomalies have solid contours, negative anomalies are dashed. Areas of significance (at the 95% level) are shaded. Cross-hatching indicates missing data.
a) warm event (El Nino) observed composite **b)** warm event (El Nino) model composite
c) cold event (La Nina) observed composite **d)** cold event (La Nina) model composite

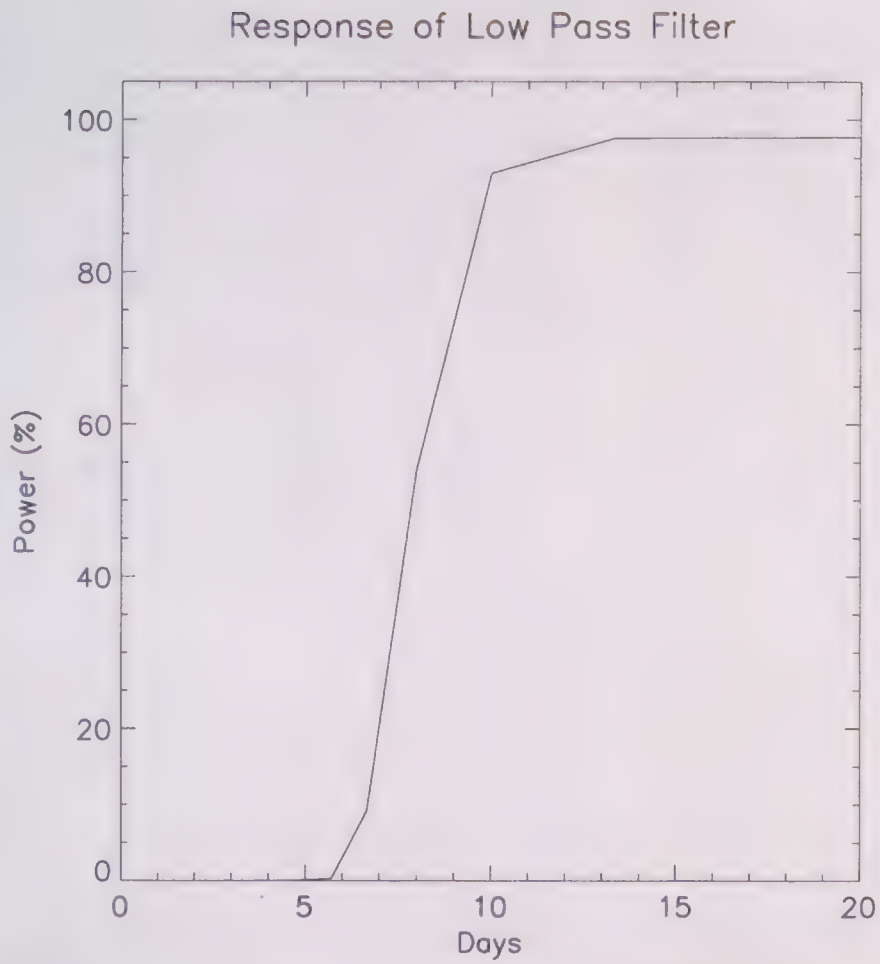

FIG. 6 Response of low-pass filter applied to daily 500 hPa height data prior to REOF analysis.

FIG. 7 Leading rotated EOFS in the NPA sector, calculated from filtered daily 500 hPa height data for JFM (1970-93).

a) Observed Pacific North American (PNA) mode
b) model PNA mode
c) Observed West Pacific (WP) mode
d) model WP mode
e) Observed East Pacific (EP) mode
f) model EP mode
g) Observed North Pacific (NP) mode
h) model NP mode

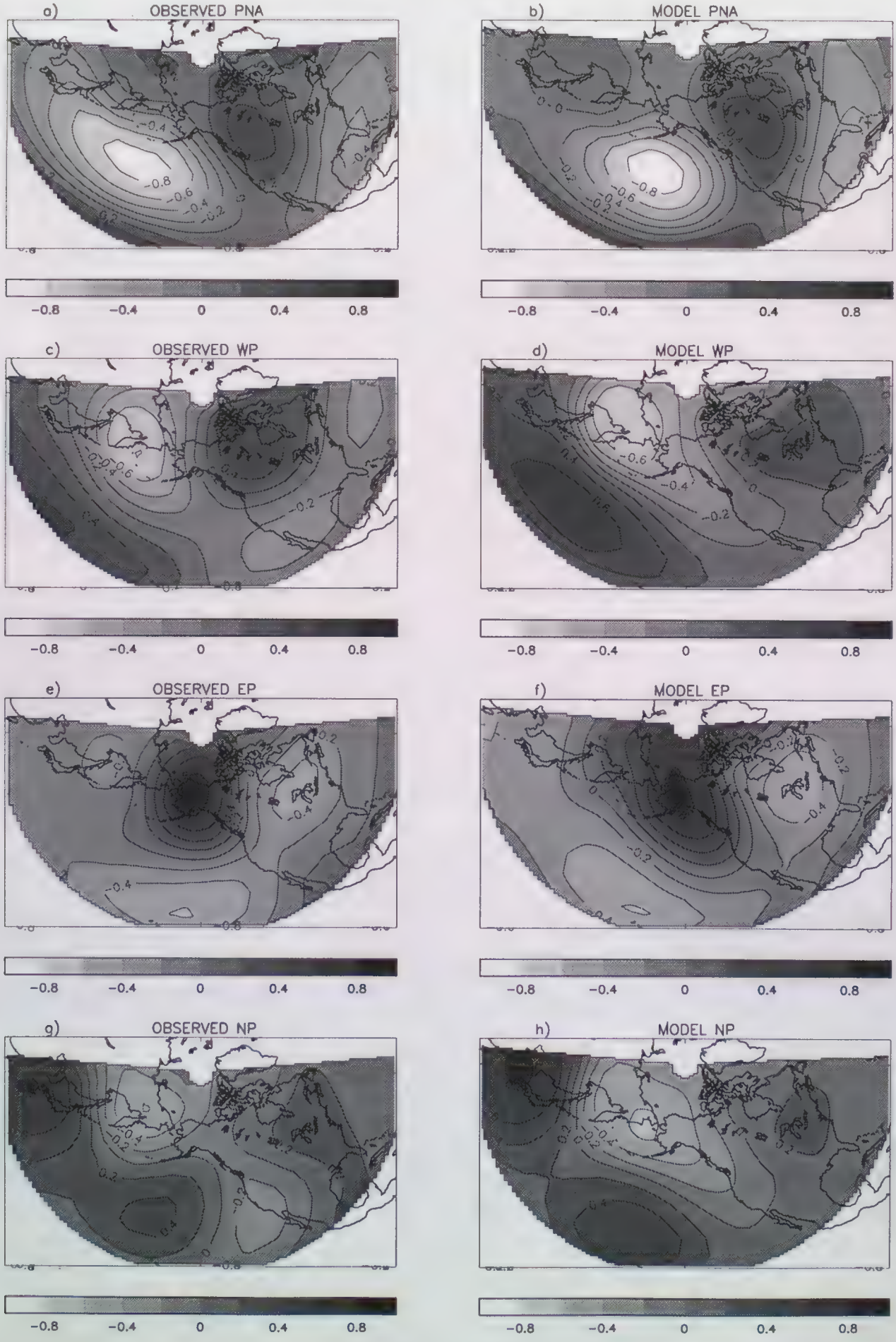

FIG. 8

a) Seasonally averaged time coefficients of the PNA mode for JFM. Each dotted line represents an individual model integration (1949-93), the dashed line is the ensemble mean, and the solid line the observed values (1968-93).

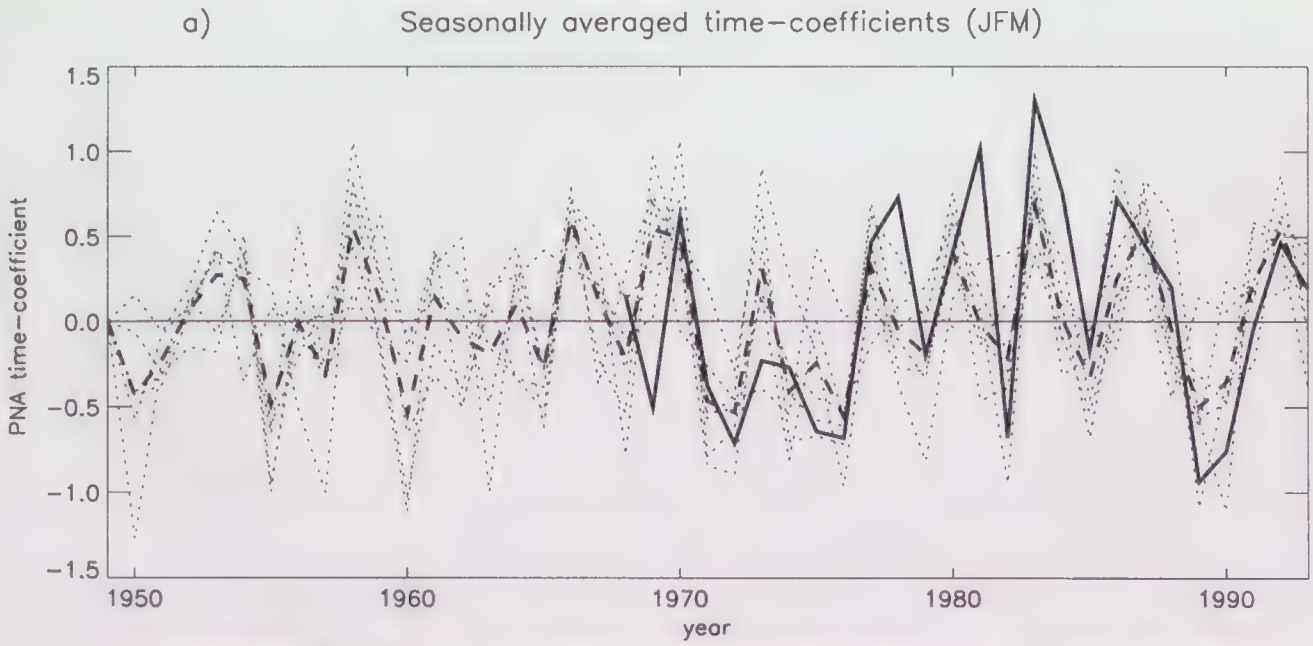

b) Correlation between GISST data and the seasonally averaged ensemble mean time-coefficients of the observed PNA mode. Solid contours indicate positive correlations, dashed contours negative. Areas of significant correlation (at the 95% level) are shaded.

c) Correlation between GISST data and the seasonally averaged time-coefficients of the model PNA mode. Shading and contours as for (b).

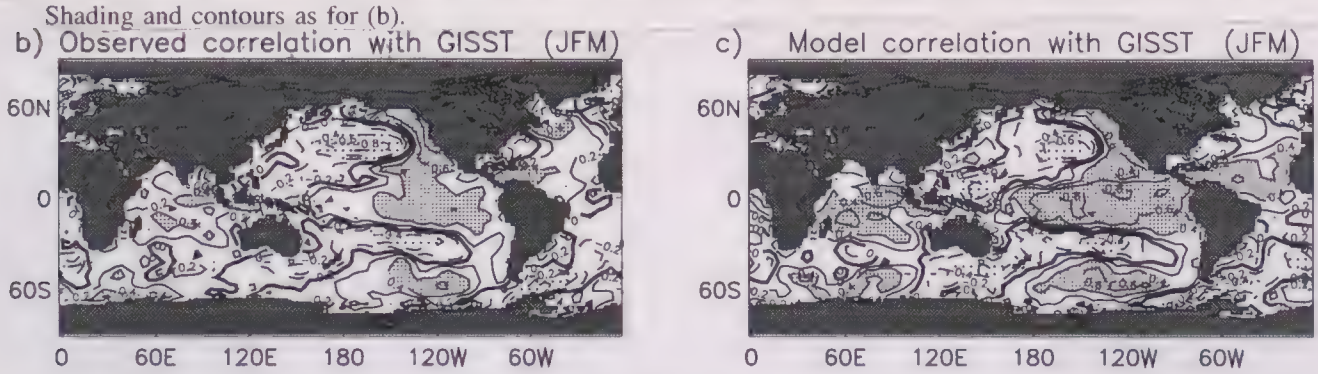

d) Probability distribution of daily time coefficients of the observed PNA mode. Solid lines are calculated using data from all years; dotted lines use data from warm event (El Nino) years; and dashed lines use data from cold event (La Nina) years.

e) as (d) but for the model PNA mode.

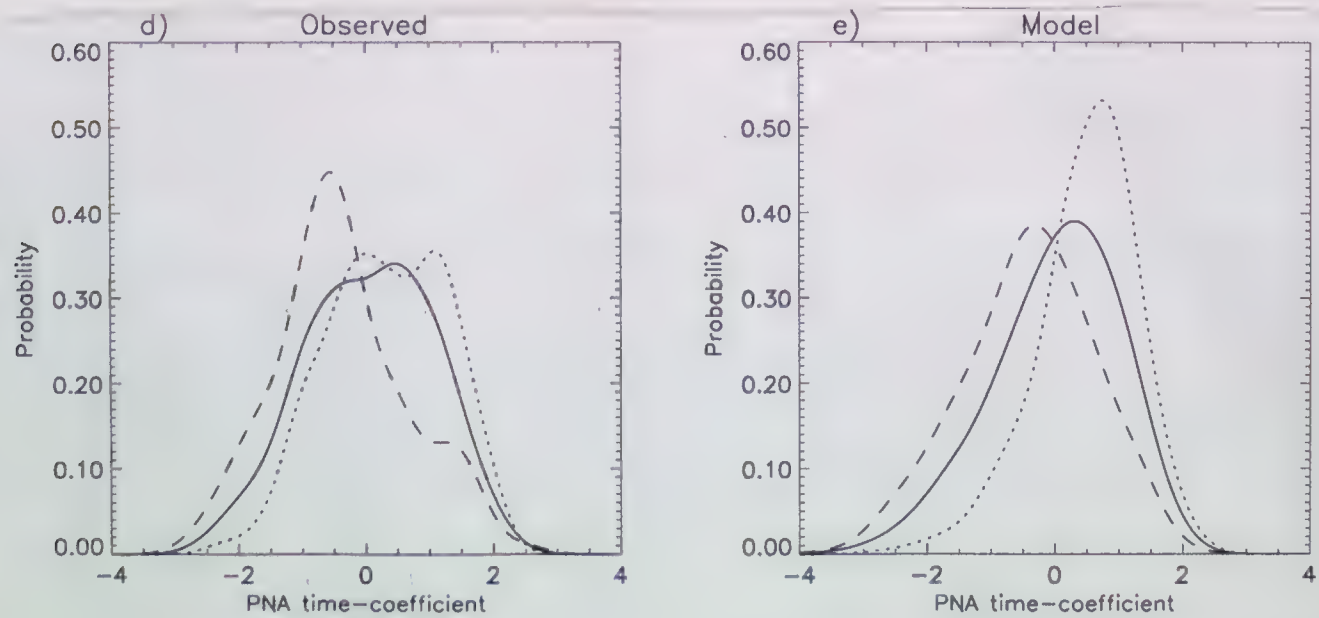

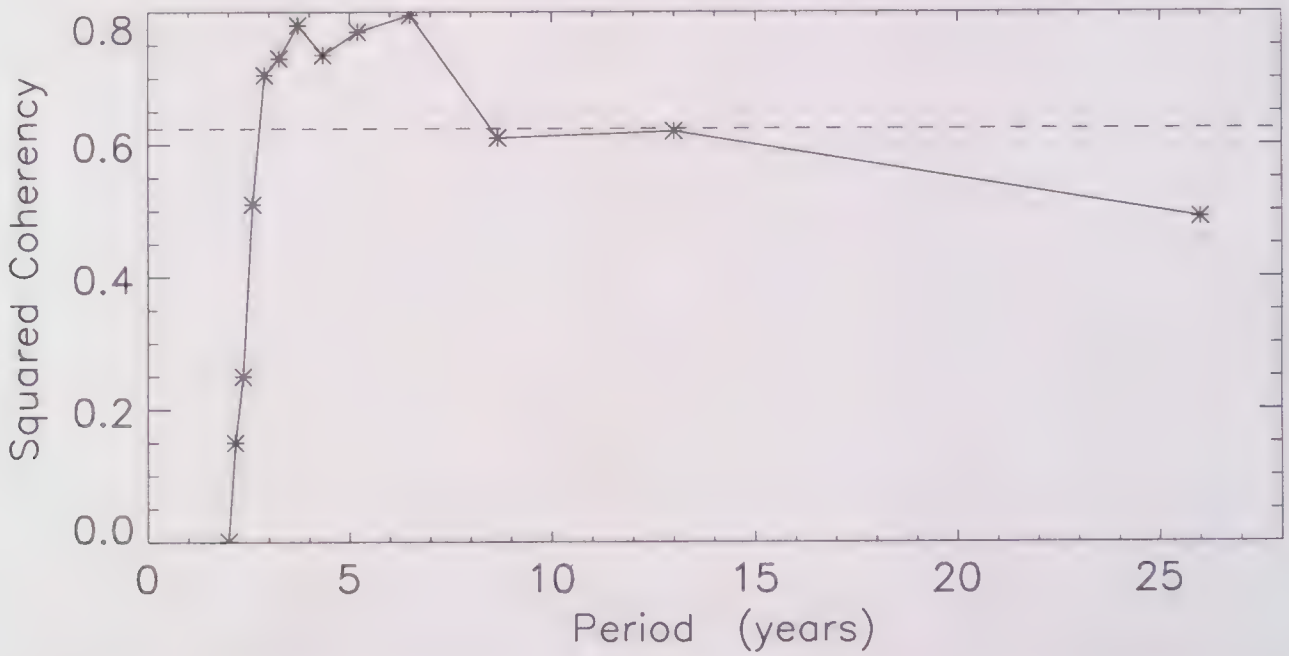

FIG. 9 Coherence between modelled and observed seasonally averaged (JFM) PNA time coefficients. Dashed line indicates 95% significance level.

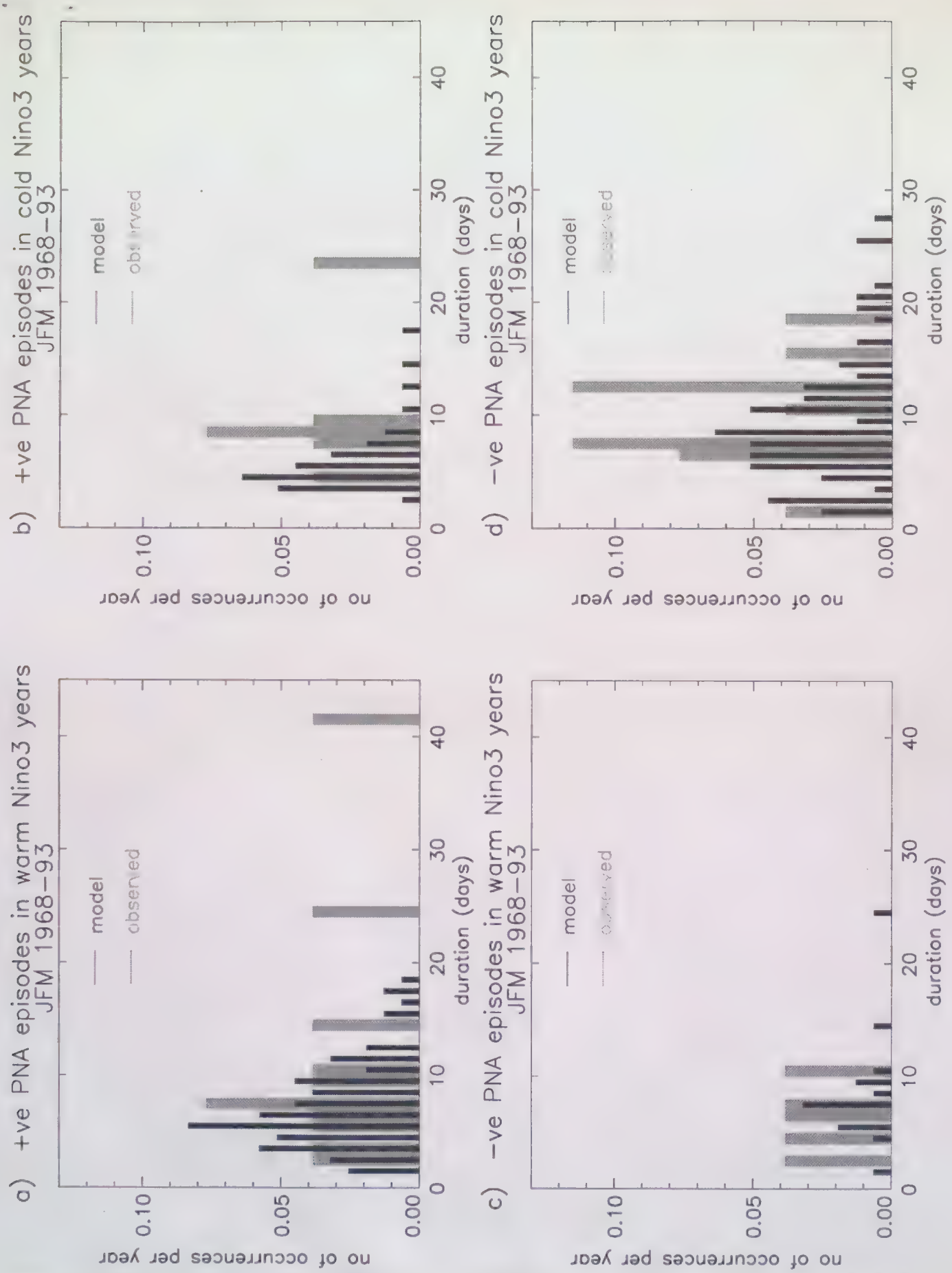

FIG. 10 Histogram of the duration of PNA episodes in JFM, 1968-93. The duration is measured as the number of consecutive whole days for which the filtered daily time coefficient exceeds |1.25| . Heavy thin bars show model values, thicker lighter bars show observed values.
a) positive PNA episodes in warm event years **b)** positive PNA episodes in cold event years
c) negative PNA episodes in warm event years **d)** negative PNA episodes in cold event years

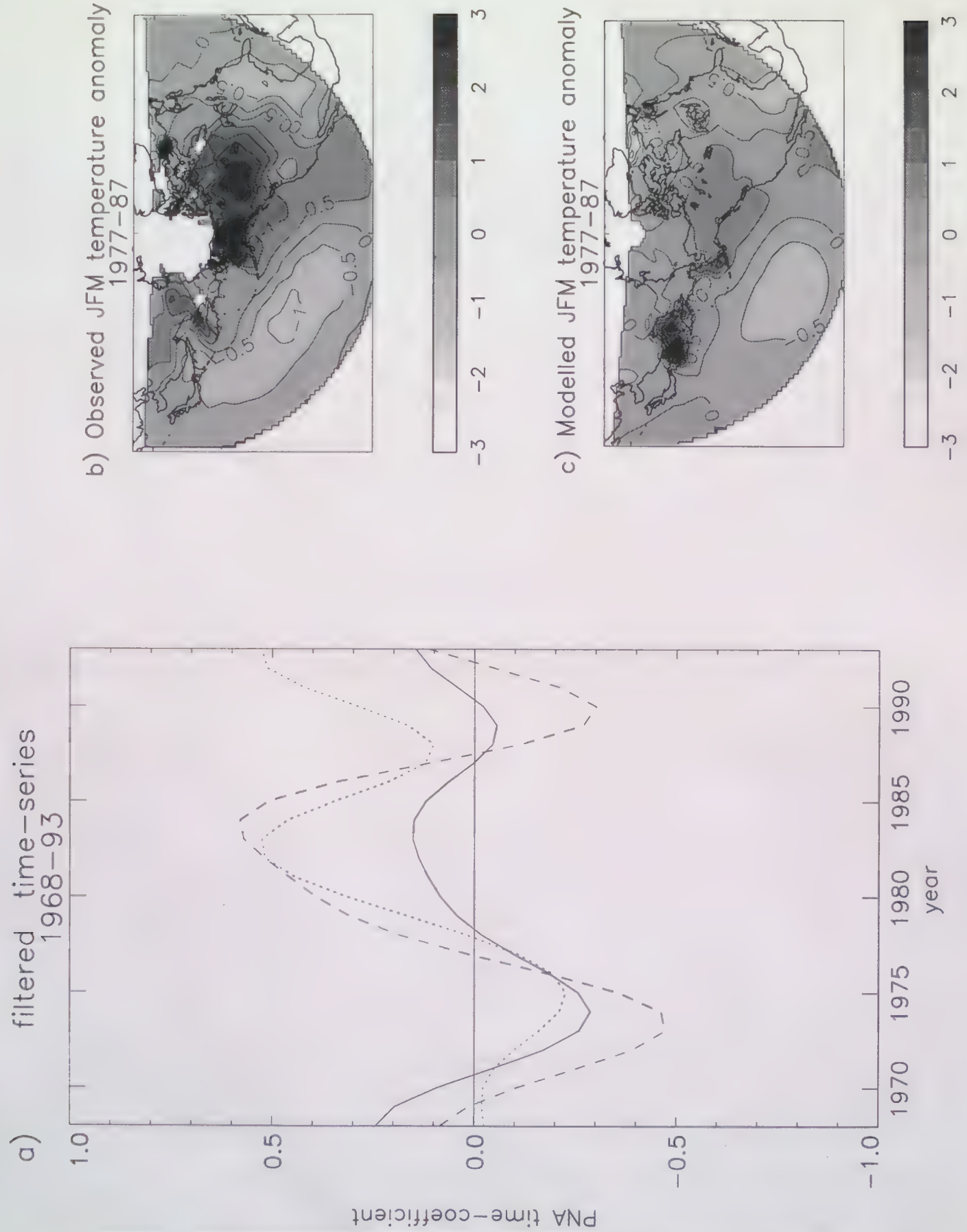

FIG. 11 a) Filtered time-series (low-pass > 8 years) showing decadal variations 1968-93. Dashed line: observed seasonally averaged (JFM) PNA time-coefficients. Solid line: modelled seasonally averaged (JFM) PNA time-coefficients. Dotted line: seasonally averaged (JFM) NINO3 SSTs. **b)** Observed and **c)** Modelled JFM decadal anomaly (1977-87) of surface air temperature in the North Pacific American region.

FIG. 12 as fig.8 but for WP mode.

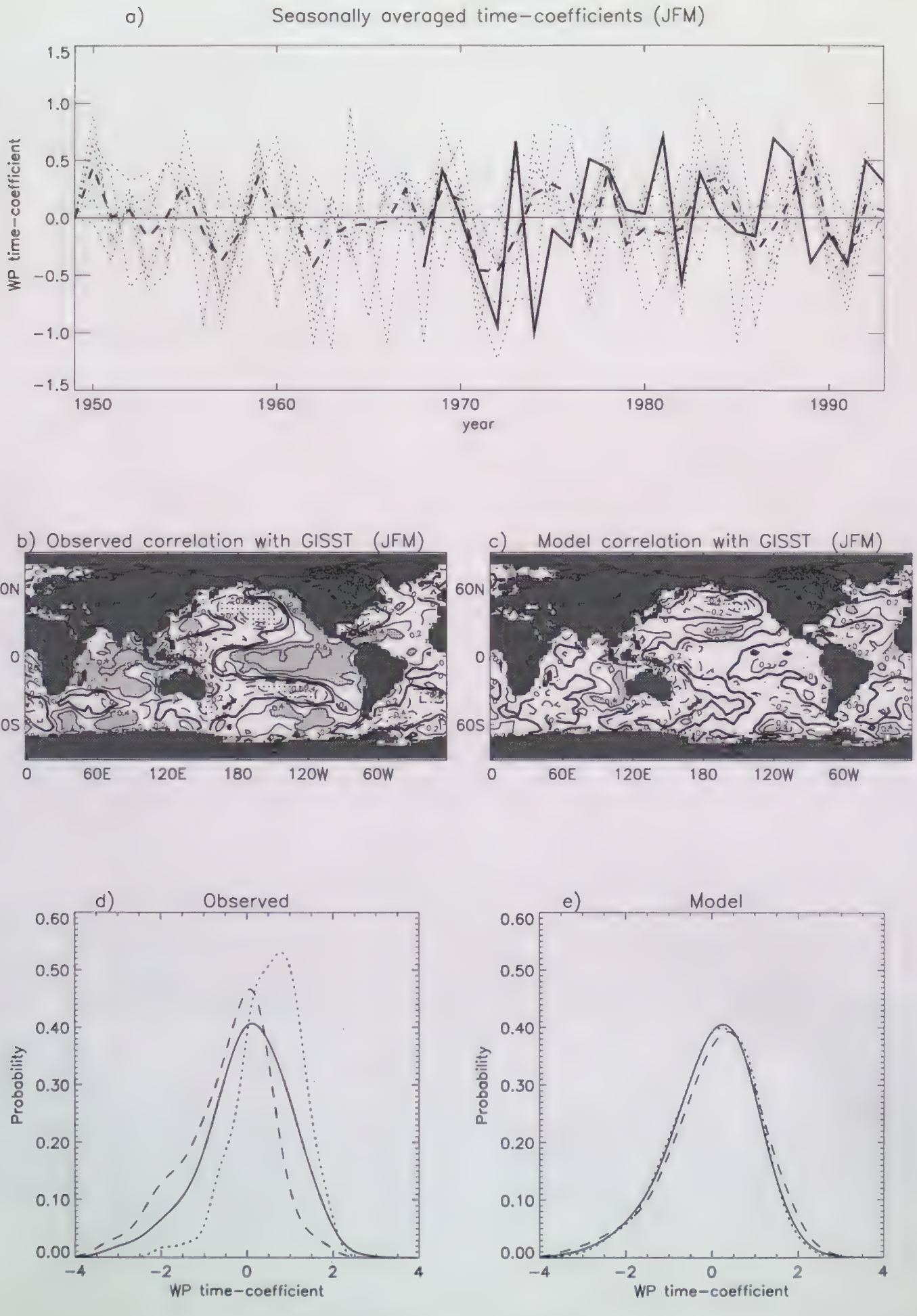

FIG. 13 as fig.8 but for EP mode.

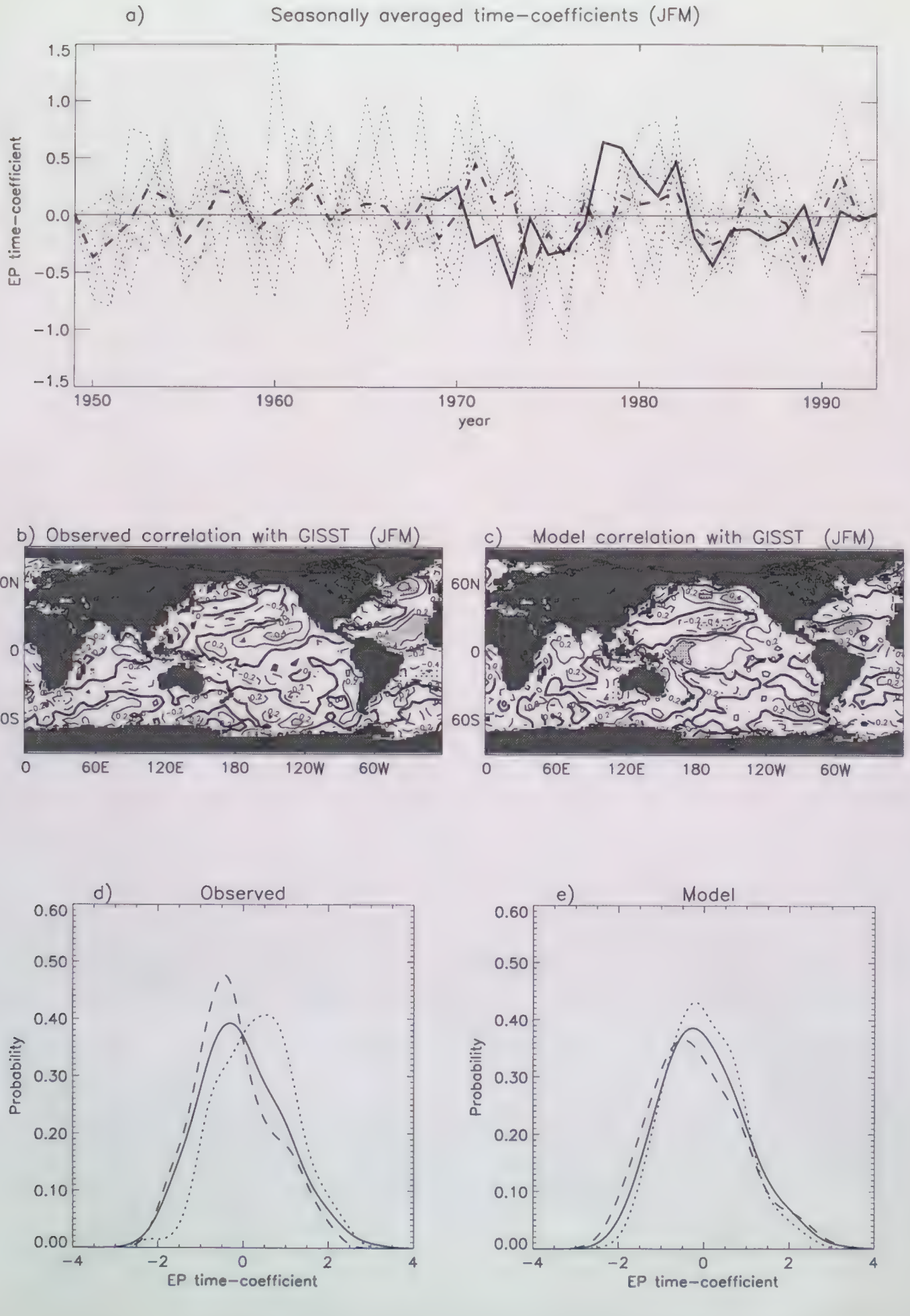

FIG. 14 as fig.8 but for NP mode.

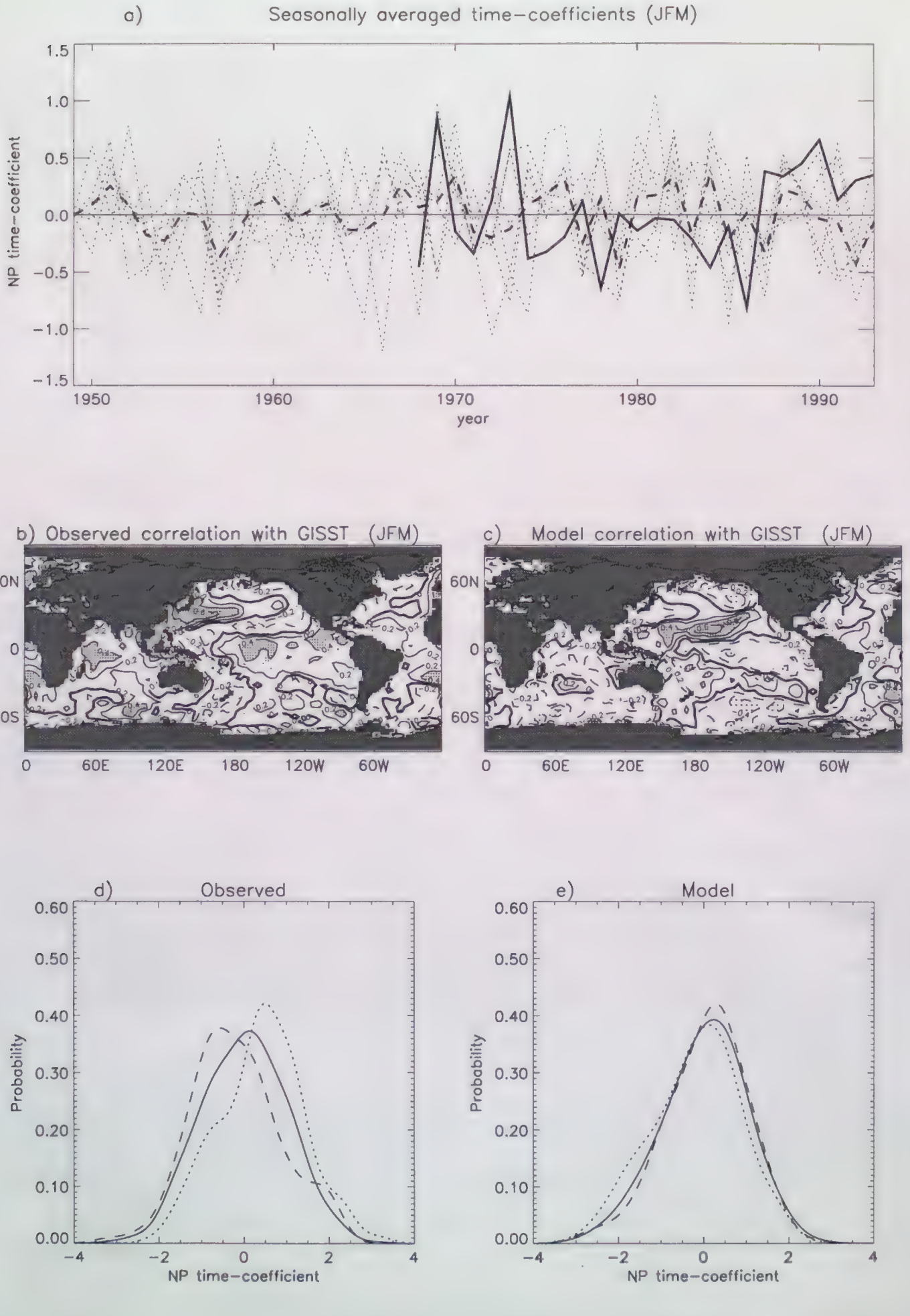

CLIMATE RESEARCH TECHNICAL NOTES

CRTN 1	Oct 1990	Estimates of the sensitivity of climate to vegetation changes using the Penman-Monteith equation. P R Rowntree
CRTN 2	Oct 1990	An ocean general circulation model of the Indian Ocean for hindcasting studies. D J Carrington
CRTN 3	Oct 1990	Simulation of the tropical diurnal cycle in a climate model. D P Rowell
CRTN 4	Oct 1990	Low frequency variability of the oceans. C K Folland, A Colman, D E Parker and A Bevan
CRTN 5	Dec 1990	A comparison of 11-level General Circulation Model Simulations with observations in the East Sahel. K Maskell
CRTN 6	Dec 1990	Climate Change Prediction. J F B Mitchell and Qing-cun Zeng
CRTN 7	Jan 1991	Deforestation of Amazonia - modelling the effects of albedo change. M F Mylne and P R Rowntree
CRTN 8	Jan 1991	The role of observations in climate prediction and research. D J Carson
CRTN 9	Mar 1991	The greenhouse effect and its likely consequences for climate change. D J Carson
CRTN 10	Apr 1991	Use of wind stresses from operational N.W.P. models to force an O.G.C.M. of the Indian Ocean. D J Carrington
CRTN 11	Jun 1991	A new daily Central England Temperature series, 1772-1991. D E Parker, T P Legg and C K Folland
CRTN 12	Jul 1991	Causes and predictability of Sahel rainfall variability. D P Rowell, C K Folland, K Maskell, J A Owen, M N Ward

CLIMATE RESEARCH TECHNICAL NOTES

CRTN 13	Jul 1991	Modelling changes in climate due to enhanced CO2, the role of atmospheric dynamics, cloud and moisture. C A Senior, J F B Mitchell, H Le Treut and Z-X Li
CRTN 14	Sep 1991	Sea temperature bucket models used to correct historical SST data in the Meteorological Office. C K Folland
CRTN 15	Aug 1991	Modelling climate change, and some potential effects on agriculture in the U.K. P R Rowntree, B A Callander and J Cochrane
CRTN 16	Aug 1991	The Boreal Forests and Climate G Thomas and P R Rowntree
CRTN 17	Aug 1991	Development of a Stratosphere-Troposphere Data Assimilation System. R Swinbank.
CRTN 18	Sep 1991	A study of asynchronous coupling using a simple climate model. M K Davey.
CRTN 19	Sep 1991	The Oceanic Carbon Cycle. N K Taylor
CRTN 20	Nov 1991	Worldwide ocean-atmosphere surface fields in Sahel wet and dry years using provisionally corrected surface wind data. M N Ward
CRTN 21	Dec 1991	Coupled tropical ocean global atmosphere models at the UKMO. M K Davey, C Gordon, S Ineson and S Lawrence
CRTN 22	Dec 1991	Empirical parameterisation of tropical ocean-atmosphere coupling. M Allen, M K Davey, D L T Anderson and P D Killworth
CRTN 23	Feb 1992	The temporal evolution of Equatorial Currents in the Indian Ocean D L T Anderson, D J Carrington, R A Corry and C Gordon
CRTN 24	Feb 1992	Stratospheric analyses provided by the U.K. Meteorological Office M J Bailey, A O'Neill and V D Pope

CLIMATE RESEARCH TECHNICAL NOTES

CRTN 25	Feb 1992	Modelling interannual variability in the Indian Ocean using momentum fluxes from the UKMO and ECMWF operational weather analyses. D L T Anderson and D J Carrington
CRTN 26	Mar 1992	A GCM simulation of the impact of Amazonian deforestation on climate using an improved canopy representation J Lean and P R Rowntree
CRTN 27	Mar 1992	The parameterization of rainfall interception in GCMs A J Dolman and D Gregory
CRTN 28	Jun 1992	Development of worldwide marine data eigenvectors since 1985 A W Colman
CRTN 29	Jun 1992	A tropical ocean model with reduced physics M K Davey
CRTN 30	Jun 1992	International Temperature Workshop, Boulder, Colorado, USA, 16 January 1992 Edited by D E Parker
CRTN 31	Jul 1992	Simulation of clear-sky outgoing longwave radiation over the oceans using operational analyses A Slingo and M J Webb
CRTN 32	Sep 1992	A prediction of the transient response of climate J M Murphy
CRTN 33	Nov 1992	LEPS scores for assessing climate model simulations and long-range forecasts. C K Folland
CRTN 34	Jan 1993	Stratospheric Data Assimilation System Guide Editer: R Swinbank
CRTN 35	Mar 1993	A Stratosphere-Troposphere Data Assimilation System R Swinbank and A O'Neill
CRTN 36	Mar 1993	Validation of hydrological schemes for climate models against catchment data. P R Rowntree and J Lean

CLIMATE RESEARCH TECHNICAL NOTES

CRTN 37	Apr 1993	Modelling of palaeoclimates: Examples from the recent past J F B Mitchell
CRTN 38	May 1993	A simulation of seasonality in ENSO forecast skill M K Davey, D L T Anderson and S Lawrence
CRTN 39	Jul 1993	ENSO Prediction experiments using a simple ocean-atmosphere model D-H Wu, D L T Anderson and M K Davey
CRTN 40	Sep 1993	Diagnosis of dynamic sea-surface and sea-level changes from the Cox ocean model J M Gregory
CRTN 41	Sep 1993	Seasonal variations of the clear-sky greenhouse effect: the role of changes in atmospheric temperatures and humidities M J Webb, A Slingo and G L Stephens
CRTN 42	Nov 1993	Sea-level changes under increasing atmospheric CO_2 in a transient coupled ocean-atmosphere GCM experiment. J M Gregory
CRTN 43	Dec 1993	Global and regional patterns of climate change: recent predictions for the Arctic P R Rowntree
CRTN 44	Feb 1994	The effect of changing horizontal diffusion in the atmospheric version of the unified climate model C D Hall and R A Stratton
CRTN 45	Mar 1994	Simulation of El-Niño/Southern Oscillation like variability in a global AOGCM and its response to CO_2 increase. S F B Tett
CRTN 46	Apr 1994	Global data required for monitoring climate change. D E Parker and C K Folland
CRTN 47	May 1994	Seasonal uptake of anthropogenic CO_2 in an ocean general circulation model. N K Taylor

CLIMATE RESEARCH TECHNICAL NOTES

CRTN 48	Jun 1994	A tropic-wide oscillation of boreal summer rainfall and patterns of sea-surface temperature. M N Ward, K Maskell, C K Folland, D P Rowell and R Washington
CRTN 49	Jun 1994	Simulation of the tropical Pacific using a simplified ocean model M A Balmaseda, D L T Anderson and M K Davey
CRTN 50	Sep 1994	Simulation of global mean temperature using a box-diffusion climate model P R Rowntree
CRTN 51	Sep 1994	Seasonal dependence of ENSO prediction skill M A Balmaseda, M K Davey and D L T Anderson
CRTN 52	Nov 1994	Simulation of the Indian Monsoon and Tropical Intraseasonal Variability by a General Circulation Model P M Inness and D Gregory
CRTN 53	Mar 1995	A comparison of modelled surface fluxes with climatological estimates. C Gordon and D K Wright
CRTN 54	Mar 1995	The representation of moist convection in atmospheric models. D Gregory
CRTN 55	Mar 1995	A consistent treatment of the evaporation of rain and snow for use in large-scale models D Gregory
CRTN 56	Apr 1995	Workshop on simulations of the Climate of the Twentieth Century using GISST, 28-30 November 1994, Hadley Centre, Bracknell, UK Edited by C K Folland and D P Rowell
CRTN 57	May 1995	Enhanced shortwave cloud radiative forcing due to anthropogenic aerosols. S E Swartz and A Slingo
CRTN 58	May 1995	The simulation of the tropical oceans in models of different horizontal resolution. C Gordon, D K Wright and C M Roberts
CRTN 59	Sep 1995	The water budget of middle latitude continental regions - a modelling and observational study P R Rowntree
CRTN 60	Sep 1995	Intraseasonal variability of the Indian summer monsoon simulated by the Hadley Centre climate model K Ashok, D Gregory and P M Inness

CLIMATE RESEARCH TECHNICAL NOTES

CRTN 61	Sep 1995	Climate simulations with the Unified Model: AMIP runs C D Hall, R A Stratton and M L Gallani
CRTN 62	Nov 1995	Validation of surface parameters over the oceans in climate simulations with the unified model. C D Hall
CRTN 63	Dec 1995	The GISST2.2 sea surface temperature and sea-ice climatology D E Parker, M Jackson and E B Horton
CRTN 64	Dec 1995	Parametrization of momentum transport by convection. II: Tests in single column and general circulation models. D Gregory, R Kershaw and P M Inness
CRTN 65	Jan 1996	Understanding the sensitivity of a GCM simulation of Amazonian deforestation to the specification of vegetation and soil characteristics. J Lean and P R Rowntree
CRTN 66	Jan 1996	On the efficient calculation of infra-red fluxes and cooling rates using the two-stream equations. J M Edwards
CRTN 67	Jan 1996	The second Hadley Centre coupled ocean-atmosphere GCM: Model description, spinup and validation. TC Johns,RE Carnell,JF Crossley,JM Gregory, JFB Mitchell,CA Senior,SFB Tett and RA Wood
CRTN 68	Feb 1996	The sensitivity of climate simulations to the specification of mixed phase clouds D Gregory and D Morris
CRTN 69	Apr 1996	Using an ensemble of Multi-Decadal GCM simulations ro assess potential seasonal predictability D P Rowell
CRTN 70	May 1996	North Atlantic and European Seasonal Predictability using an Ensemble of Multi-Decadal AGCM Simulations J R Davies, D P Rowell and C K Folland
CRTN 71	Jun 1996	A description of the Second Hadley Centre Coupled Model (HADCM2) T C Johns
CRTN 72	Jul 1996	Palaeoclimate Modelling Intercomparison: UKMO GCM simulations for 6kBP and 21kBP C D Hewitt and J F B Mitchell

CLIMATE RESEARCH TECHNICAL NOTES

CRTN 73 Aug 1996 ENSO responses and low frequency weather variability in the North Pacific/American sector 1949-93

A C Renshaw, D P Rowell and C K Folland